

Response to Reviewers' comments

We appreciate the re-reviews by Anonymous Reviewers #2 and #3. Please see below our response (in blue) to their comments (in black).

Reviewer #2:

I would suggest accepting contingent on the following minor corrections:

L44-45: “full source contribution”: the meaning is not altogether clear. I assume you mean zeroing-out the emissions.

Added: “(i.e., based on 100% emission perturbation)”

L45: “to a 20%” should be “from a 20%”

We changed the “obtained by” to “obtained from”. The “to” before “a 20%” goes with “sensitivities”.

L47: the meaning of O3 sensitivities is not clear here

It means: sensitivities to a 20% reduction in the EAS anthropogenic emissions. This has been clarified.

L50-51: I would remove the list of possible differences between HTAP1 and HTAP2 results. This list is not all inclusive (for example it could be due to different models or different model designs etc). It is sufficient, especially in the abstract to say they are different.

We deleted the list here in the abstract per your suggestion, but added “a number of reasons including” before this list in the conclusion. “the different experiment designs of HTAP1 and HTAP2” we include in this list contains the meaning of “different models or different model designs etc”.

L177: Goal 1. This goal cannot be realized due to the long list of caveats that the authors have listed. It is probably necessary to run one model configuration from the HTAP1 focus time-period to that of HTAP2 to understand how the LRT impacts change through time. I would suggest changing this goal to comparing the different results between HTAP1 and HTAP2.

The suggestion of “run one model configuration from the HTAP1 focus time-period to that of HTAP2 to understand how the LRT impacts change through time” is great, and it will very likely be accounted for in future studies as discussed at an HTAP2 related workshop at the US EPA. We changed the language to “comparing the differences in..., which could help..”.

L201: “Identical” seems a bit strong here due to ambiguities in VOC speciation. The speciation is discussed to some extent further down in the manuscript. It would seem relevant to discuss the VOC speciation in this section.

We agree that the VOC speciation was treated differently by each model. “Identical” here refers to whatever in the provided format, and for NMVOCs meaning the total amount.

L229-230: Biogenic emissions are tacked on here almost as an afterthought, but are discussed in more detail below. It would make sense to include a section on differences in non-anthropogenic

emissions and to condense discussion on them. A little detail is given on the supplement for some of the models for non-anthropogenic NO_x emissions. Why are STEM lightning NO_x emissions offshore masked out? Why are the emissions differences not characterized over a broader domain (as the paper seems to imply much of the difference in the model sensitivities are due to domain boundary conditions)? Why are differences in isoprene emissions not given? It seems that a simple table in the supplement could encapsulate some of the differences in non-anthropogenic emissions between the different models in different source areas.

The materials regarding non-anthropogenic NO_x emissions also supported the discussions of OMI/GEOS-Chem NO₂ comparison, and therefore both their spatial distributions and regional total amounts are useful for this paper. We use GEOS-Chem and STEM non-anthropogenic NO_x emission comparisons as an example to make the point that the differences among individual models for individual species/source types are big, partially affecting the model performance. The comparison of GEOS-Chem and STEM were initially done to support Lapina et al. (2014), for which biogenic isoprene emissions were not compared. As we mentioned, non-anthropogenic emissions from all models by species/source types should be quantified and summarized in future studies. STEM offshore lightning NO_x emissions (which were much smaller than over land and many were in pollution export regions) were masked out as at that time we in general have higher confidence in the WRF precipitation over land. Their impacts on the modeled O₃ inland are expected to be small.

L253: What is the “NAMALL” simulation? It does not seem to follow the naming convention.

L253: Please specify explicitly what “GLO” stands for.

NAM means the North America source region as shown in Figure 1. We now specified below the equations that “GLO” stands for the “global” source region.

L269: Please make the notation in equation (2) consistent with the notation above. In (2) some terms are written as subscripts while above they are written above in parenthesis (i.e., term 2). Term 3 seems to exclude the “-20%” in some places.

Done.

L558: Are you sure the NO_x emissions are overestimated? Doesn't the paper state above that it is not straightforward to draw conclusion with respect to emissions from satellite measurements.

Changed to “the uncertainties in”.

L657: Please revisit the Brown-Steiner and Hess paper. After looking at their paper I do not see that they claim a factor of 3 between summer and other seasons.

These refer to results in their Table 2 (US) and 3 (North America) for Spring (MAM) and Summer (JJA) ratios.

L760-763: Please rephrase. I do not understand this point very well from what is written.

It now reads as: “Therefore, the R(MDA8, EAS, 20%) values shown in Figure 10 during the model-based periods of O₃ exceedances can represent the sensitivities during the actual periods of O₃ compliance in non-western US regions, and may not represent the sensitivities during all actual O₃ exceedances in the western US.”

L914: “continently”

Changed to “conveniently calculating”.

L879-883: I would change “due” to “due in part”. This list is not really complete giving all the differences why these values may differ.

Changed to “due to a number of reasons including...”

Reviewer #3

The authors have addressed most of my major concerns, and I list below additional suggestions for the authors to strengthen the paper a bit more before publication. The abstract and conclusions could better convey the main findings from the paper. For example, I was surprised that the findings from Figures 10 and 11 aren't discussed.

We added a sentence in the abstract regarding Figure 10-11 findings “The EAS pollution impacts are weaker during observed O₃ exceedances than on all days in most US regions except over some high terrain western US rural/remote areas.” The paragraph in conclusion starting from L908 discusses about these as well.

L47 not clear what the sensitivities are to (Asian emissions?)

Added: “to the 20% EAS emission perturbations”

L58-60 is confusing as these events aren't occurring at the same times in the eastern US as in the western US. How much did stratospheric and transported EAS pollution influence US ozone during these events?

Referring to at satellite overpass times. Satellite data were used to identify these episodes, distinguish LRT/stratospheric intrusions, and evaluate models, but not to quantify the contributions from each sources.

L498-500 Can you say anything about what this finding implies regarding problems with the model simulations?

We just described the changes in smaller magnitude than in the western US (of >10 ppbv), which was discussed in earlier sentences.

L598-601 is confusing as Mexico is usually considered part of North America. From Figure 1 it's clear that it is separate, but this might be worth pointing out here.

We added: “(not included in the NAM source regions, see Figure 1)”

L626 stronger-than-normal-transport from where to where? And compared to what time period (i.e., what is normal?)?

Added: “trans-Pacific”. And “stronger-than-normal” was changed to “stronger” to compare 2010 (HTAP2) conditions with 2000/2001 (HTAP1).

L643-644. Given the comparison with observations, is this estimate expected to be too high or better than the other models?

We do not intend to evaluate the sensitivities here.

L659. Why is nonlinear O₃ chemistry stronger outside of summer?

As a reflection of seasonal transition of chemical regime. See more discussions in Wu et al. (2009), Fiore et al. (2009), and Brown-Steiner and Hess (2011) on the ozone responses to NO_x or/and NMVOC perturbation results for earlier years.

L697-698, also repeated L741-742 and 915-916. How exactly will the new satellite help capture high O₃ and LRT events? Does it have better sensitivity of ozone near the surface?

We emphasize the benefit from future geostationary satellite's better spatial coverage in smaller footprint sizes (2-5 km). The more frequent sampling than the polar-orbiting satellites is also beneficial. Multi-spectral retrievals would have better sensitivity than single-spectral retrievals in general. A more recent paper on TEMPO was now cited.

L734 Are the PBL depths higher during the LRT episodes? This would help to convince the reader of this interpretation.

The sentence near L734 is on PBLH's diurnal variability. This question is also worth some investigation. We correlated the daily daytime mean WRF PBLH with the STEM EAS influences throughout the period (8 May-30 June) to evaluate the relationships between daily variability of PBLH and the EAS source influences. Only in certain regions, we see medium/strong positive correlations ($r > 0.5$), where the PBL depths were higher during the LRT episodes, as the correlations may have been complicated by the relationships between PBLHs-local influences. Some earlier sentences in this paragraph were modified to include this finding.

L744-749. It seems the important message here is that EAS typically isn't contributing to the highest days, yet this doesn't come out til 2 paragraphs later and didn't seem to be highlighted in the abstract or conclusions. The exception of the few sites in the southwestern U.S. in L768-772 is also important to note, and it'd be even better if these impacts are quantified in the abstract/conclusions. Are these sites at higher elevation? It might be worth to report separately high elevation sites from the rest of the western sites.

The paragraph starting from L744 describes Figure 10, which is based on modeled exceedances in all grids. The results here are contrasted with Figure 11 in the following paragraphs to show the impacts of spatial coverage and the biases in modeled exceedances on determined R values. As we mentioned near L770, many of the western sites in Figure 11d-f are at high terrain (Figure 2a; regional mean model/actual elevation in Table 3) rural/remote areas where local influences are less dominant, but it does not seem that the differences between the sensitivities on all days and during exceedances are higher at higher elevation sites (e.g., Colorado contrasting with Arizona and Utah sites as shown in Figure 11).

L794-799. Were these captured in the Lin et al. 2012ab studies? Wondering if this applies to all global models or just the ones used here.

Here we draw these conclusions based only on the three boundary condition models used in this study, not including the AM3 model which was used in Lin et al. (2012a,b). All models included in this study (here and throughout the paper) are those that have data available in the AeroCom database submitted following HTAP2 data submission procedure.

At Grand Canyon NP, Lin et al. (2012a,b)'s AM3 results showed positive ozone biases with a moderate model/observation correlation of 0.49 during spring/summer 2010 (See Lin et al., 2012b, Figure 9, upper-right panel) and time-shifted ozone anomaly around 9 May 2010 (See Lin et al.,

2012a, Figure 11, mid panel). However, we do not find evaluation of AM3 O₃ vertical distributions around 9 May in their papers, and the published Lin et al. (2012a,b) results are not based on HTAP2 emission inputs.

L808. Unless the stratospheric contribution was diagnosed in the model, this attribution to stratospheric is speculative and should be clarified as such or deleted. Is the assimilation only assimilating stratospheric ozone or total ozone? Is it somehow tracking stratospheric ozone? “Such as” was changed to “possibly including”. MLS O₃ is from UTLS and above; OMI O₃ is total.

L822 should be clearer that it influenced mid-tropospheric ozone over the Northeast.
Modified as suggested.

L828-831. Are the mixing depths shallower here and thus don't entrain as much free tropospheric ozone into the surface layer?

Yes, it does seem that the modeled PBLHs over these regions during the event are shallower than over the western US in the daytime, so this might be a reason as well. However, please note our reply to your earlier comment on L734 regarding PBLH-EAS/local influences relationships. The related sentence has been modified.

L863-868 Why not discuss the contribution to events here?

Contributions during events are discussed in a later paragraph (~L908). This paragraph focuses on the monthly mean results from STEM and its boundary condition models, as well as from the multi- models.

L871 How many global models?

Changed to “eight”.

L874-875. It's not clear if this bottom up NO_x inventory discussion applies globally or to certain regions

In global models, globally; in STEM, just within its regional domain.

L885-886. Is this the forward model GEOS-Chem or the adjoint sensitivities?

From the GEOS-Chem adjoint model v35f (initially developed from standard GEOS-Chem v8-02-01 with many updates ever since, details at: http://adjoint.colorado.edu/~yanko/gcadj_std/GC_adj_man.pdf), based on the emission perturbation approach. We cited findings from the adjoint sensitivities in Lapina et al. (2014).

L922 and elsewhere – use of “free-running”. Does this mean the models are generating their own weather and thus not expected to match specific observations? I think the authors mean simply that they aren't doing chemical data assimilation, but I'm not sure if this is the accepted use of this term.

We added: “(i.e., without chemical data assimilation)” for clarity. Also changed in the abstract.

1 **Impact of Intercontinental Pollution Transport on North American Ozone Air Pollution:**
2 **An HTAP Phase 2 Multi-model Study**

3
4 Min Huang^{1,2}, Gregory R. Carmichael³, R. Bradley Pierce⁴, Duseong S. Jo⁵, Rokjin J. Park⁵,
5 Johannes Flemming⁶, Louisa K. Emmons⁷, Kevin W. Bowman⁸, Daven K. Henze⁹, Yanko Davila⁹,
6 Kengo Sudo¹⁰, Jan Eiof Jonson¹¹, Marianne Tronstad Lund¹², Greet Janssens-Maenhout¹³,
7 Frank J. Dentener¹³, Terry J. Keating¹⁴, Hilke Oetjen^{8,*}, Vivienne H. Payne⁸

8
9 ¹George Mason University, Fairfax, VA, USA

10 ²University of Maryland, College Park, MD, USA

11 ³University of Iowa, Iowa City, IA, USA

12 ⁴NOAA National Environmental Satellite, Data, and Information Service, Madison, WI, USA

13 ⁵Seoul National University, Seoul, Korea

14 ⁶European Center for Medium range Weather Forecasting, Reading, UK

15 ⁷National Center for Atmospheric Research, Boulder, CO, USA

16 ⁸Jet Propulsion Laboratory, California Institute of Technology, Pasadena, CA, USA

17 ⁹University of Colorado-Boulder, Boulder, CO, USA

18 ¹⁰Nagoya University, Furocho, Chigusa-ku, Nagoya, Japan

19 ¹¹Norwegian Meteorological Institute, Oslo, Norway

20 ¹²Center for International Climate and Environmental Research, Oslo, Norway

21 ¹³European Commission, Joint Research Center, Ispra, Italy

22 ¹⁴US Environmental Protection Agency, Washington, DC, USA

23 *Now at: University of Leicester, Leicester, UK

24
25 *Correspondence to:* Min Huang (mhuang10@gmu.edu)

26 **Abstract**

27

28 The recent update on the US National Ambient Air Quality Standards of the ground-level
29 ozone (O₃) can benefit from a better understanding of its source contributions in different US
30 regions during recent years. In the Hemispheric Transport of Air Pollution experiment Phase 1
31 (HTAP1), various global models were used to determine the O₃ source-receptor relationships
32 among three continents in the Northern Hemisphere in 2001. In support of the HTAP Phase 2
33 (HTAP2) experiment that studies more recent years and involves higher-resolution global models
34 and regional models' participation, we conduct a number of regional scale Sulfur Transport and
35 dEposition Model (STEM) air quality base and sensitivity simulations over North America during
36 May-June 2010. STEM's top and lateral chemical boundary conditions were downscaled from
37 three global chemical transport models' (i.e., GEOS-Chem, RAQMS, and ECMWF C-IFS) base
38 and sensitivity simulations in which the East Asian (EAS) anthropogenic emissions were reduced
39 by 20%. The mean differences between STEM surface O₃ sensitivities to the emission changes
40 and its corresponding boundary condition model's are smaller than those among its boundary
41 condition models, in terms of the regional/period mean (<10%) and the spatial distributions. An
42 additional STEM simulation was performed in which the boundary conditions were downscaled
43 from a RAQMS simulation without EAS anthropogenic emissions. The scalability of O₃
44 sensitivities to the size of the emission perturbation is spatially varying, and the full (i.e., based on
45 100% emission perturbation) source contribution obtained from, linearly scaling the North
46 American mean O₃ sensitivities to a 20% reduction in the EAS anthropogenic emissions may be
47 underestimated by at least 10%. The three boundary condition models' mean O₃ sensitivities to
48 the 20% EAS emission perturbations are ~8% (May-June 2010)/~11% (2010 annual) lower than
49 those estimated by eight global models, and the multi-model ensemble estimates are higher than
50 the HTAP1 reported 2001 conditions. GEOS-Chem sensitivities indicate that the EAS
51 anthropogenic NO_x emissions matter more than the other EAS O₃ precursors to the North
52 American O₃, qualitatively consistent with previous adjoint sensitivity calculations.

53 In addition to the analyses on large spatial/temporal scales relative to the HTAP1, we also
54 show results on subcontinental- and event-scale that are more relevant to the US air quality
55 management. The EAS pollution impacts are weaker during observed O₃ exceedances than on all
56 days in most US regions except over some high terrain western US rural/remote areas. Satellite O₃
57 (TES, JPL-IASI, and AIRS) and carbon monoxide (TES and AIRS) products, along with surface
58 measurements and model calculations, show that during certain episodes stratospheric O₃
59 intrusions and the transported EAS pollution influenced O₃ in the western and the eastern US
60 differently. Free-running (i.e., without chemical data assimilation) global models underpredicted
61 the transported background O₃ during these episodes, posing difficulties for STEM to accurately
62 simulate the surface O₃ and its source contribution. Although we effectively improved the modeled
63 O₃ by incorporating satellite O₃ (OMI and MLS) and evaluated the quality of the HTAP2 emission
64 inventory with the KNMI OMI nitrogen dioxide, using observations to evaluate and improve O₃
65 source attribution still remains to be further explored.

Deleted: by

Deleted: .

Deleted: multiple

Deleted: , due to the growing EAS anthropogenic emissions, the interannual variability in atmospheric circulation (i.e., stronger trans-Pacific transport in spring 2010 following an El Niño event), and the different experiment designs of HTAP1 and HTAP2.

74 **1. Introduction**

75

76 Tropospheric ozone (O₃), a short-lived trace gas with a lifetime ranging from hours in the
77 boundary layer to weeks in the free troposphere, affects tropospheric chemistry, harms human and
78 ecosystem health, and induces climate change on local, regional and global scales (Jerrett et al.,
79 2009; Smith et al., 2009; Anenberg et al., 2010; Mauzerall and Wang, 2001; Avnery et al., 2011a,
80 b; Shindell et al., 2009, 2013; Bowman and Henze, 2012; Stevenson et al., 2006, 2013; Monks et
81 al., 2015). It has been recognized that the uneven distributions of tropospheric O₃ can be attributed
82 to the stratosphere as well as local, regional and distant emission sources, through complicated
83 processes that occur on synoptic, meso- and micro-scales (Task Force on Hemispheric Transport
84 of Air Pollution (HTAP), 2010; National Research Council (NRC), 2009; Maas and Grennfelt,
85 2016). The mitigation of O₃'s climate and health impacts would benefit from efforts to control the
86 emissions of its precursors from the various emission sources (United Nations Environment
87 Programme (UNEP) and World Meteorological Organization (WMO), 2011), such as nitrogen
88 oxides (NO_x), carbon monoxide (CO), methane (CH₄), and non-methane volatile organic
89 compounds (NMVOCs).

90

91 Ground-level O₃ is one of the six criteria air pollutants regulated by the US Environmental
92 Protection Agency (EPA), and the US National Ambient Air Quality Standards (NAAQS) has
93 recently been lowered to 70 ppbv to better protect Americans' health and the environment. Issues
94 regarding making accurate estimates of the total O₃ as well as the background O₃ level (defined as
95 the concentration that is not affected by recent locally-emitted or produced anthropogenic pollution)
96 (e.g., McDonald-Buller et al., 2011; Zhang et al., 2011; Fiore et al., 2014; Huang et al., 2015),
97 have been recently discussed as part of the implementation of the new US O₃ standard (US EPA,
98 2016a, b). This includes assessing the impacts of various components of the background O₃, such
99 as stratospheric O₃, local natural sources such as biogenic, lightning and wildfire emissions, as
100 well as the long-range transport (LRT) of pollution. The impact of the trans-Pacific pollution
101 transport on US air quality has been evaluated in numerous studies over the past decades (e.g.,
102 Fiore et al., 2009; Reidmiller et al., 2009; Zhang et al., 2008, 2009; Huang et al., 2010, 2013a; Lin
103 et al., 2012a, 2015, 2016; US EPA, 2016a). It has been found that the increasing trends of pollution
104 in the upwind continents, especially the populated East Asia (e.g., Zhang et al., 2014; Susaya et
105 al., 2013; Wang et al., 2012), may partially offset the US air quality improvements in recent
106 decades due to the regional and local emission controls (e.g., Jacob et al., 1999; Verstraeten et al.,
107 2015; Ambrose et al., 2011; Wigder et al., 2013; Cooper et al., 2010; Parrish et al., 2009, 2012;
108 Gratz et al., 2014). A better understanding of the processes that determine the O₃ pollution levels,
109 as well as an improved capability of attributing the air pollution to nearby or distant sources is
110 needed to assist with designing and implementing effective local emission control strategies to
111 comply with the tighter air quality standards.

112

113 Chemical transport models are often used to reproduce and attribute the observed O₃ levels,
114 including assessing the impacts of the internationally transported O₃ on the US air quality. In the
115 HTAP modeling experiment Phase 1 (HTAP1), various global models with horizontal resolutions
116 ranging from 1°×1° to 5°×5°, only around half of which are finer than 3°×3°, were used to
117 determine the O₃ source-receptor (SR) relationships among three continents in the Northern
118 Hemisphere in 2001 (Chapter 4 in HTAP, 2010). The global model based SR relationships in
119 HTAP1 determined using the emission perturbation approach (i.e., calculating the changes of O₃

120 at the receptor regions in response to a 20% reduction in the emission inputs in a given source
121 region) were reported as either monthly 24h mean values or policy-relevant metrics such as the
122 maximum daily 8h average (MDA8) for the US (e.g., Fiore et al., 2009; Reidmiller et al., 2009).
123 Large intermodel diversity was found in the simulated total O₃ and the intercontinentally
124 transported pollution for the chosen SR pairs in the northern midlatitudes, indicating the challenges
125 with model simulations to accurately represent the key atmospheric processes. Multi-model mean
126 results were the foci of in these studies with the assumption that this approach can reduce the
127 uncertainty from the single model estimates for monthly or seasonal means. “Ensemble” model
128 analyses have been suggested by some US stakeholders as one of the methods for helping with the
129 characterization of the background O₃ components (US EPA, 2016b). Although the multi-model
130 approach can help identify some of the weaknesses of the individual models and may produce
131 more reliable estimates, it is necessary to well understand the uncertainties inherent in using the
132 same set of anthropogenic emissions in all these model simulations. Satellite observations over the
133 regions with limited in-situ measurements such as the East Asia can be particularly helpful for
134 quantifying such uncertainties.

135
136 The 20% emission perturbation in the HTAP1 modeling experiment was chosen to produce
137 a sizeable (i.e., larger than numerical noise) and realistic impact, but small enough in the assumed
138 near-linear atmospheric chemistry regime. The scalability of the modeled O₃ sensitivities to the
139 size of the emission perturbations has been assessed on continental scale (Wu et al., 2009; Fiore et
140 al., 2009; HTAP, 2010; Wild et al., 2012; Emmons et al., 2012). The receptor O₃ responses to the
141 source-region emission perturbations are found to be fairly linear within ~50% of the perturbations.
142 However, due to the chemical non-linearity, the full source contribution obtained by linearly
143 scaling the receptor regional mean O₃ sensitivity to the 20% reduction in the source region
144 emissions may be underestimated, and the scalability depended on seasons and the perturbed
145 emission species. Huang et al. (2013b) investigated the scalability of the O₃ sensitivity between
146 the southern California-US intermountain west SR pair for May 2010, in which study the southern
147 California anthropogenic emissions were perturbed by multiple amounts of +50%, -50%, -100%.
148 They reported that the scalability of the O₃ sensitivities changed with the distance from the source
149 regions. Further analyses on the scalability of these modeled O₃ sensitivities during recent years
150 especially for the East Asia-NAM SR pair, as well as their spatial variability, are still needed.
151 Furthermore, results generated using the emission perturbation approach need to be compared with
152 those based on the other methods (e.g., tagged tracers, adjoint sensitivity).

153
154 Previous studies have demonstrated the advantages of high resolution chemical transport
155 modeling for understanding SR relationships (e.g., Lin et al., 2010 for Europe and the East Asia;
156 Lin et al., 2012a; Huang et al., 2010, 2013a for Asia and NAM). Using observations (satellite,
157 sondes, aircraft) along with single model simulations, a few studies have reported that the US O₃
158 sensitivities to extra-regional sources is time- and region-dependent (e.g., Lin et al., 2012a, b;
159 Langford et al., 2011; Ott et al., 2016), and therefore the necessity of evaluating the extra-regional
160 source impacts on event scale has been emphasized in these studies as well as in US EPA (2016a,
161 b). The HTAP Phase 2 (HTAP2) multi-model experiment, initiated in 2012, is designed to advance
162 the understanding of the impact of intercontinental pollution transport during more recent years
163 (i.e., 2008-2010) involving a number of global and regional models’ participation (Galmarini et
164 al., 2017; Koffi et al., 2016). The regional models are anticipated to help connect the analyses over
165 global and regional scales and enable discussions on small spatial (e.g., subcontinental) and

166 temporal scales (i.e., event based analyses). The use of satellite products for identifying the
167 transport events as well as for quantitative model evaluation is also encouraged in the work plan.
168 The HTAP2 modeling experiment was sequentially conducted in two steps. First, similar to the
169 HTAP1 experiment, a group of global models with different resolutions conducted base and
170 emission perturbation sensitivity simulations to determine the pollutants' SR relationships. All
171 models in their base simulations used the same set of harmonized sector-based global
172 anthropogenic emissions developed specifically for the HTAP2 modeling experiment (Janssens-
173 Maenhout et al., 2015). Most of these global models recorded only key chemical species from their
174 base and sensitivity simulations in varied temporal frequencies. Several global models saved the
175 three-dimensional (3D) chemical fields of more species with a 3- or 6-hour interval, which are
176 suitable for being used as regional models' chemical boundary conditions. In the second step,
177 regional models conducted base and sensitivity simulations to analyze the pollutants' SR
178 relationships in greater detail. The regional model simulations used the same set of anthropogenic
179 emissions as the global models within their simulation domains, and the chemical boundary
180 conditions in these regional simulations were downscaled from the base and sensitivity simulations
181 from the selected boundary condition model outputs. For regional simulations over the North
182 America and Europe, boundary conditions were mostly taken from a single model such as the
183 ECMWF C-IFS or GEOS-Chem.

184
185 This study aims to address: 1) comparing the differences in O₃ sensitivities generated from
186 the HTAP2 and HTAP1 experiments, which could help address how the LRT impacts on NAM
187 changed through time; 2) how the refined modeling experiment design in HTAP2 can help advance
188 our understanding of the LRT impacts on NAM, particularly the involvement of regional models
189 and the inclusion of small spatial/temporal scale analysis during high O₃ episodes that are more
190 relevant to air quality management; 3) the usefulness of satellite observations for better
191 understanding the sources of uncertainties in the modeled total O₃ (e.g., from the emission and
192 regional models' boundary condition inputs) as well as for reducing the uncertainties in some of
193 these model inputs via chemical data assimilation. We performed a number of regional scale
194 STEM (Sulfur Transport and dEposition Model) base and sensitivity simulations over the NAM
195 during May-June 2010, during which period strong trans-Pacific pollution transport were shown
196 to episodically impact the US (Lin et al., 2012a). Extending the HTAP2 regional simulations' basic
197 setup, the STEM top and lateral chemical boundary conditions were downscaled from three global
198 models' (i.e., the Seoul National University (SNU) GEOS-Chem, RAQMS, and the ECMWF C-
199 IFS) base and sensitivity simulations in which the East Asian anthropogenic emissions were
200 reduced. The STEM surface O₃ sensitivities over the NAM region based on different boundary
201 condition models were inter-compared, in terms of the regional averages and the spatial patterns
202 on monthly basis and during a selected event identified by satellite O₃ and CO products. These
203 were also compared with the sensitivities estimated by their corresponding boundary condition
204 models as well as all HTAP2 participating global models and the results from HTAP1.

206 2. Methods

207 2.1. Anthropogenic emission inputs

208
209 Identical anthropogenic emissions were used in all global and regional chemical transport
210 models' base and sensitivity simulations. This monthly-varying harmonized sectoral (i.e., power,
211 industry, transportation, residential, shipping, aircraft, agriculture) emission inventory was

Deleted: to

213 provided on a gridded $0.1^\circ \times 0.1^\circ$ resolution for the years of 2008 and 2010, by compiling the
214 officially reported emissions at the national scale (Janssens-Maenhout et al., 2015;
215 http://edgar.jrc.ec.europa.eu/htap_v2). The temporal profiles for developing the monthly-varying
216 emissions differ by region and sector. The amount of emissions of key O₃ precursors (CO, NO_x,
217 NMVOCs) from both years are summarized in Table S1 for the four major emissions sectors, over
218 the NAM (US+Canada, based on data from the US EPA and the Environmental Canada, which
219 shows lower emissions from the previous years as also discussed in Pouliot et al., 2015), MICS-
220 Asia regions (south, southeast, and east Asia, based on country inventory for China and from the
221 Clean Air Policy Support System and the Regional Emission inventory in ASia 2.1, more
222 information also in Li et al., 2017), and for over the world. For all of these species, global total
223 emissions in 2008 and 2010 are similar. The NO_x, NMVOC, and CO emissions decreased from
224 2008 to 2010 over the NAM by 10.7%, 9.4%, and 15.7%, respectively. In 2008, NAM NO_x,
225 NMVOC and CO contributed to 18.0%, 11.7% and 11.9% of the global total, respectively, and in
226 2010, these contributions became 15.8%, 10.5% and 10.2%. For 2010, the transportation sector
227 contributed more than the other sectors to NAM anthropogenic NO_x and CO emissions; industrial
228 sector contributed more than the other sectors to NMVOCs emissions. Over East Asian countries,
229 these emissions are ~2-5 times higher than the US emissions, and the NO_x, NMVOC and CO
230 emissions increased over Asia by 7.3%, 7.2% and 1.0%, with the dominant emission sectors in
231 2010 of transportation, industry, and residential, respectively. For both years, the emissions over
232 the MICS-Asia regions contribute to over 40% of the global emissions. For these key O₃ precursors,
233 the East Asian countries contribute to 45% (NMVOCs)-70% (NO_x) of the emissions in the MICS-
234 Asia domain in both years, and the south Asian countries contribute to ~22% (NO_x)-34%
235 (NMVOCs) of the MICS-Asia emissions. The uncertainty of the emission estimates differs by
236 emission sector and species: i.e., the emissions from large-scale combustion sources (e.g., NO_x
237 and CO from power and industry sectors) are less uncertain than those from small-scale and
238 scattered sources (e.g., CO and NMVOCs from transportation and residential sources). Non-
239 anthropogenic emission inputs used in different models' simulations may differ, and their impacts
240 on the modeled total O₃ and the SR relationships will be compared in detail in future studies.

241 2.2. *Region definitions for the SR study and the model base and sensitivity simulations*

242 2.2.1. Base and 20% emission perturbation simulations from global and regional models

243 The HTAP2 simulations from eight global models, used in this study, are listed in Table
244 1a, including the relevant references. Horizontal and vertical resolutions of these models range
245 from finer than 1° to coarser than 2.5° , and from 20 to 60 layers, respectively. Overall these
246 resolutions are higher than the HTAP1 participating models'. Figure 1 defines the source regions
247 used in the HTAP2 SR relationship study and we will focus in this study on assessing the East
248 Asia (EAS), S Asia (SAS), Europe (EUR), and non-NAM anthropogenic source (interchangeable
249 in this paper with "(all) foreign") impacts on the NAM O₃ levels in 2010. Specifically, each model
250 performed a base simulation and a number of sensitivity simulations in which the original HTAP2
251 anthropogenic emissions for all species and sectors in a defined source region were perturbed by
252 a certain amount (referring to 20% as in most cases) and these cases are defined in Table 1a-b as
253 **source region*ALL(*perturbation*)*, where "ALL" refers to "all species and sectors", consistent
254 with HTAP1 and HTAP2's naming convention. The O₃ differences $R(O_3, \textit{*source region*},$
255 $\textit{*perturbation*})$ over the NAM were then calculated between each model's base and sensitivity
256 simulations:
257
258

259 $R(O_3, EAS, 20\%) = \text{BASE } O_3 - \text{EASALL}(-20\%) O_3$ (1a)
 260 $R(O_3, SAS, 20\%) = \text{BASE } O_3 - \text{SASALL}(-20\%) O_3$ (1b)
 261 $R(O_3, EUR, 20\%) = \text{BASE } O_3 - \text{EURALL}(-20\%) O_3$ (1c)
 262 $R(O_3, \text{non-NAM}, 20\%) = \text{NAMALL}(-20\%) O_3 - \text{GLOALL}(-20\%) O_3$ (1d)

263 Where “GLO” stands for the “global” source region.

Deleted:
Formatted: Subscript

264
 265 The monthly-mean $R(O_3, \textit{source region}^*, 20\%)$ values were averaged over the NAM
 266 region for the analysis and compared with the findings in the HTAP1 study (e.g., Fiore et al., 2009).
 267 It is worth mentioning that the rectangular source regions defined in HTAP1 were modified in
 268 HTAP2 to align with the geo-political borders. For EAS and SAS, the regions not overlapped by
 269 HTAP1 and HTAP2 are mostly in the less populated/polluted regions such as the northwestern
 270 China, according to the HTAP2 emission maps (http://edgar.jrc.ec.europa.eu/htap_v2/index.php).
 271 HTAP2's EUR domain excludes certain regions in Russia/Belarus/Ukraine, Middle East and
 272 North Africa that are included in HTAP1's EUR domain. The impact of emissions over these
 273 regions on comparing the NAM $R(O_3, EUR, 20\%)$ values in HTAP1 and HTAP2 will be discussed
 274 in Section 3.2.1.

275
 276 A unitless “Response to Extra-Regional Emission Reductions (RERER)” metric
 277 (Galmarini et al., 2017), as defined in eq. (2), was also calculated to measure the importance of
 278 local versus non-local sources to NAM's O_3 levels:

279
$$\text{RERER}(O_3, \text{NAM}) = \frac{R(o_3, \text{non-NAM}, 20\%) - (\text{NAMALL}(-20\%) O_3 - \text{GLOALL}(-20\%) O_3)}{R(o_3, \text{global}, 20\%) - (\text{BASE } O_3 - \text{GLOALL}(-20\%) O_3)} \quad (2)$$

Deleted: $\frac{R_{O_3, \text{non-NAM}, 20\%}}{R_{O_3, \text{global}, 20\%}} = \frac{(\text{NAMALL } O_3 - \text{GLOALL } O_3)}{(\text{BASE } O_3 - \text{GLOALL } O_3)}$
Formatted: Left

280 The denominator and numerator terms of RERER represent the impacts of global and non-NAM
 281 anthropogenic emissions on NAM O_3 , respectively. The higher the NAM RERER value is, the
 282 stronger impact from non-local sources on NAM is indicated. The RERER value can exceed 1,
 283 when emission reductions led to increasing concentrations (e.g. O_3 titration by nitrogen monoxide
 284 (NO)).

285
 286 The STEM (version 2K3) regional simulations were then performed on a 60 km×60 km
 287 horizontal resolution (a typical coarse regional model resolution) grid over NAM within the
 288 domain defined in Figure 2a during May-June 2010. The meteorological conditions in spring 2010
 289 were compared with the climatology from the NCEP/NCAR reanalysis data for the 1981-2010
 290 period (Kalnay et al., 1996) in Huang et al. (2013b), concluding that this spring represents a period
 291 of stronger-than-climatological average spring trans-Pacific transport, based on a stronger
 292 meridional gradient in the North Pacific and higher Pacific/North American (PNA) indexes. This
 293 is consistent with the findings by Lin et al. (2014) that the El Niño conditions during the 09/10
 294 winter strengthened the trans-Pacific transport of Asian pollution in spring 2010. The mean near-
 295 surface air temperatures in the western US in this spring were lower than the climatology, with
 296 larger anomalies in the mountain states, which may have led to weaker local O_3 production and
 297 decomposition of the transported peroxyacyl nitrates (PAN). In contrast, higher-than-normal
 298 temperatures were found in the eastern US that favored anomalously strong local O_3 production.

299
 300 STEM has been used to interpret the observations collected by satellites and during aircraft
 301 campaigns in the past decade (e.g., Carmichael et al., 2003a, b; Huang et al., 2010, 2013a, b, 2014,
 302 2015). STEM calculates gas-phase chemistry reactions based on the SAPRC 99 gaseous chemical
 303 mechanism (Carter, 2000) with thirty photolysis rates calculated online by the Tropospheric
 304 Ultraviolet-Visible radiation model (Madronich et al., 2002). Most of the key configurations of the

307 60 km base simulations are the same as those described in Lapina et al. (2014), i.e., meteorological
308 fields were pre-calculated by the Advanced Research Weather Research and Forecasting Model
309 (WRF-ARW, Skamarock et al., 2008) version 3.3.1 forced by the North American Regional
310 Reanalysis data (Mesinger et al., 2006), using a similar set of the physics configuration to those in
311 Huang et al. (2013a). Biomass burning emissions are from the Fire INventory from NCAR (FINN)
312 inventory version 1.0 (Wiedinmyer et al., 2011). Biogenic emissions were calculated by the Model
313 of Emissions of Gases and Aerosols from Nature (MEGAN) version 2.1 (Guenther et al., 2012),
314 driven by the WRF meteorology. Lightning NO_x emissions are generated following the method in
315 Allen et al. (2012), with the flash rates determined by the WRF convective precipitation and scaled
316 to the National Lightning Detection Network flash rates. A major difference of the STEM
317 simulations in this study from the Lapina (2014) study is that the anthropogenic emissions were
318 replaced with the monthly-mean HTAP2 inventory with no weekday-weekend variability applied,
319 rather than the earlier National Emission Inventory (NEI) 2005 in which the weekday-weekend
320 variability exists. This change can introduce uncertainty for some US regions where weekday-
321 weekend variability of some O₃ precursors' emissions was notable during the studied period (e.g.,
322 weekend NO_x emissions in southern California during spring/summer 2010 were 0.6-0.7 of the
323 weekday emissions as reported by Kim et al. (2016) and Brioude et al. (2013)), but this was done
324 to ensure consistency with the HTAP2 global model simulations, that also didn't use daily variable
325 emissions for any regions in the world. The VOC speciation for the SPRAC 99 chemical
326 mechanism in the NEI 2005 (ftp://aftp.fsl.noaa.gov/divisions/taq/emissions_data_2005) were
327 applied to break down the total NMVOC emissions provided in the HTAP2 inventory. The VOC
328 speciation based on the year of 2005 can be unrealistic for 2005 as well as 2010 as studies have
329 reported variable temporal changes of different VOC species in some US cities (e.g., Warneke et
330 al., 2012). The time-varying lateral and top boundary conditions in the STEM base simulations
331 were downscaled from three global models (i.e., 3 hourly SNU GEOS-Chem, 3 hourly ECMWF
332 C-IFS, and 6 hourly RAQMS) base simulations. In support of the SR relationship study to quantify
333 the East Asia anthropogenic impacts on the NAM, three STEM sensitivity simulations were also
334 conducted in which the STEM boundary conditions were downscaled from the EASALL(-20%)
335 sensitivity simulations by these three global models (Table 1b). All STEM simulated 3D chemical
336 fields were saved hourly for the convenience of calculating the US primary O₃ standard metric
337 MDA8 as well as the quantitative comparisons against the satellite Level 2 (L2) O₃ products. The
338 STEM base case surface O₃ performance and its O₃ sensitivities were also compared with those of
339 its boundary condition models as well as the multi- global model means. The latitude/longitude
340 ranges (20-50°N/130-65°W) of NAM for the global and regional model based sensitivity
341 calculations were selected to mainly account for the coverage of the STEM domain, which are
342 slightly different from the definition of North America in HTAP1.

343
344 Note that non-anthropogenic emission inputs used in STEM and its boundary condition
345 models differed, as summarized in Table 1c. Figure S1 shows detailed comparisons between
346 STEM and GEOS-Chem's non-anthropogenic (i.e., soil, lightning, biomass burning) NO_x
347 emission inputs, and their impacts on the modeled NAM background O₃ were included in Lapina
348 et al. (2014). Such quantitative comparisons will also be carried out between STEM and its other
349 boundary condition models in future studies.

350
351 2.2.2. Additional base and sensitivity simulations from selected models
352

353 In addition to the base and 20% EAS all-category emission perturbation simulations, the
354 global RAQMS model conducted a sensitivity simulation in which the East Asian anthropogenic
355 emissions were zeroed out, which was also used as STEM's boundary conditions (Table 1b). We
356 calculate the "S_{O₃}" metric (eq. (3)) using the O₃ sensitivities in STEM and RAQMS at the receptor
357 regions in response to both 20% and 100% of emission reductions, to explore the relationships
358 between the O₃ sensitivity and the size of the emission perturbation. A closer-to-one "S_{O₃}" value
359 indicates higher scalability of the sensitivity based on the 20% emission perturbation method for
360 obtaining the full "contribution" of the East Asian anthropogenic emissions on the NAM O₃.

$$361 S_{O_3} = R(O_3, \text{EAS}, 100\%) / R(O_3, \text{EAS}, 20\%) / 5 \quad (3)$$

362
363 Where: $R(O_3, \text{EAS}, 100\%) = \text{BASE } O_3 - \text{EASALL}(-100\%) O_3$

364
365 The RAQMS model also provided a base simulation that assimilated satellite O₃ products
366 from the Ozone Monitoring Instrument (OMI, Levelt et al., 2006) and Microwave Limb Sounder
367 (MLS, Livesey et al., 2008) (Pierce et al., 2007), which was used to help better understand the
368 regional model base run error sources, as well as for demonstrating the use of satellite observations
369 to help improve the representation of the trans-boundary pollution.

370
371 We also used a number of sensitivity simulations produced by the GEOS-Chem adjoint
372 model v35f in which the emissions from selected anthropogenic emission sectors (power&industry,
373 transportation, residential) or individual O₃ precursor chemical species (NO_x, VOC, CO) over the
374 East Asia were reduced by 20%. Additional simulations for the 2008-2009 periods by the SNU
375 GEOS-Chem were also utilized to quantify the East Asia and non-NAM anthropogenic source
376 impacts in comparison with the 2010 conditions that we mainly focus on in this study.

377 2.3. *In-situ and satellite observations*

379 2.3.1. *In-situ observations*

380 Over the receptor NAM, the hourly O₃ observations at the Clean Air Status and Trends
381 Network (CASTNET, <http://epa.gov/castnet/javaweb/index.html>) sites were used to evaluate the
382 global and regional models' base simulations in four subregions: western US (i.e., the EPA regions
383 8, 9, 10); southern US (i.e., the EPA regions 4 and 6), the Midwest (i.e., the EPA regions 5 and 7),
384 and the northeast (i.e., the EPA regions 1-3). The numbers of sites used in global and regional
385 models' evaluation in each US subregion are summarized in Tables 2-3. The locations of these
386 sites and the subregions they belong to are indicated in Figure 2a, overlaid on a model-based terrain
387 height map. A majority of the CASTNET sites in the western US are located at high elevation (>1
388 km) remote or rural regions, more susceptible to the trans-boundary pollution (e.g., Jaffe, 2011).
389 Most of the sites in the other three subregions are located in low elevation regions, mainly affected
390 by local and regional pollution. The model-based terrain heights fairly well represent the reality
391 on subregional scale – the differences between the actual and model-based subregional mean
392 terrain heights at the CASTNET sites are smaller than 0.1 km (Table 3).

393
394 During May-June 2010, intense ozonesonde measurements were made at multiple
395 California locations (Cooper et al., 2011), in support of the NOAA "California Nexus (CalNex):
396 Research at the Nexus of Air Quality and Climate Change" field experiment (Ryerson et al., 2013).
397 They have been used to evaluate the simulated O₃ vertical profiles by the HTAP2 participating

398 models. The detailed evaluation results have been shown by Cooper et al. (2016), and will be
399 covered by subsequent publications.

400

401 Over HTAP2's EAS source region, the global models' O₃ performance was evaluated
402 against the monthly-mean surface in-situ O₃ measurements at 11 sites within the Acid Deposition
403 Monitoring Network in East Asia (EANET, <http://www.eanet.asia>) that had data throughout the
404 year of 2010. These include eight Japanese and three Korean sites (Figure 3a), all of which are
405 located at low elevation regions (2-150 m). The reported monthly mean observations at these sites
406 were based on weekly or daily sampled data, varying among sites.

407

408 2.3.2. Satellite products

409

410 In two case studies of high O₃ episodes, L2 and L3 O₃ and CO retrievals from several
411 satellite instruments were used to assess the impacts of trans-Pacific pollution transport and
412 stratospheric O₃ intrusions on NAM O₃ levels in early May. These include: 1) the early afternoon
413 O₃ and CO profiles version 5 from the Tropospheric Emission Spectrometer (TES) (Beer et al.,
414 2001; Beer, 2006) on the Aura satellite; 2) the mid-morning O₃ profiles from the METOP-Infrared
415 Atmospheric Sounding Interferometer (IASI), which were retrieved using the Jet Propulsion
416 Laboratory (JPL) TES optimal estimation retrieval algorithm (Bowman et al., 2006) for selected
417 areas including the western US (Oetjen et al., 2014, 2016); as well as 3) the early afternoon L3 O₃
418 and CO maps (version 6, 1°×1°) from the Aqua Atmospheric Infrared Sounder (AIRS) instrument.
419 The TES tropospheric O₃ retrieval is often sensitive to the mid- to lower free troposphere, and O₃
420 at these altitudes in the Eastern Pacific is known to possibly impact the downwind US surface air
421 quality at later times (Huang et al., 2010; Parrish et al., 2010). TES O₃ is generally positively
422 biased by <15% relative to high accuracy/precision reference datasets (e.g., Verstraeten et al.,
423 2013). Although IASI is in general less sensitive than TES due to its coarse spectral resolution, the
424 681–316 hPa partial column-averaged O₃ mixing ratios in the JPL product agree well with TES
425 O₃ for the 2008–2011 period with a -3.9 ppbv offset (Oetjen et al., 2016). Note that IASI O₃ data
426 are processed operationally in Europe using a different algorithm. For this work we used O₃
427 profiles from TES and IASI processed using a consistent algorithm at JPL, although the latter set
428 of data represents only a small subset of the full set of the IASI radiance measurements. The IASI
429 and TES L2 O₃ profiles (screened by the retrieval quality and the C-Curve flags) were used to
430 evaluate the STEM O₃ vertical distributions in the different base simulations, and the satellite
431 observation operators were applied in these comparisons. Taking TES as an example, its
432 observation operator h_z for O₃ is written in (4):

$$433 \quad h_z = z_c + A_{\text{TES}} (\ln(F_{\text{TES}}(c)) - z_c) \quad (4)$$

434 where z_c is the natural log form of the TES constraint vector (a priori) in volume mixing ratio.
435 A_{TES} is the averaging kernel matrix reflecting the sensitivity of retrieval to changes in the true state
436 (Rodgers, 2000). F_{TES} projects the modeled O₃ concentration fields c to the TES grid using spatial
437 and temporal interpolation. The exponential of h_z is then used to compute the mismatches between
438 the model and TES O₃ retrievals as the model evaluation. A small mismatch between model with
439 the satellite observation operators and the satellite retrievals may indicate either good model
440 performance or may be the low sensitivity of the retrievals to the true O₃ profile. AIRS O₃ is
441 sensitive to the altitudes near the tropopause, with positive biases over the ozonesondes in the
442 upper troposphere (e.g., Bian et al., 2007); AIRS CO is most sensitive to 300–600 hPa (Warner et
443 al., 2007) and is frequently used together with the AIRS O₃ to distinguish the stratospheric O₃

444 intrusions from long-range transported anthropogenic or biomass burning pollution. We use the
445 L3 AIRS products in this study to get a broad overview of the areas that are strongly impacted by
446 the stratospheric O₃ intrusions or/and LRT of pollution.

447
448 The bottom-up NO_x emissions from the HTAP2 inventory were assessed on a monthly base
449 by comparing the GEOS-Chem nitrogen dioxide (NO₂) columns with the de-striped KNMI (Royal
450 Netherlands Meteorological Institute) OMI column NO₂ product version 2.0 (Boersma et al.,
451 2011a, b). For this model evaluation against the OMI L2 products, the NO₂ fields calculated by the
452 GEOS-Chem adjoint model were saved daily at 13:30 local solar time, roughly coinciding with
453 the Aura and Aqua overpassing times. Other parameters used in the model column calculations
454 came from the GEOS-5/GEOS-Chem monthly mean conditions. The OMI data that passed the
455 tropospheric quality flag at 13-14 local time were selected based on the following screening criteria:
456 surface albedo<0.3; cloud fraction<0.2; solar zenith angle <75°; and viewing zenith angle <45°.
457 The averaging kernels (Eskes and Boersma, 2003) and Air Mass Factors (AMFs) in the KNMI
458 product were used to calculate the modeled tropospheric NO₂ vertical columns comparable to the
459 OMI's. Details of the method to compare the model-based NO₂ columns with the KNMI OMI's
460 can be found in Huang et al. (2014).

461 3. Results and Discussions

462 3.1. Evaluation of the HTAP2 bottom-up NO_x emissions and the model base simulations

463 3.1.1. Evaluation of the bottom-up NO_x emissions

464
465
466 The comparison of the GEOS-Chem adjoint NO₂ columns with the OMI product was used
467 to help assess the bottom-up HTAP2 NO_x emissions. Figure 4 shows that NO₂ columns from
468 GEOS-Chem's base simulations over the US are overall overestimated. While grid-scale
469 differences in NO₂ columns may not be directly indicative of emissions biases (Qu et al., 2016),
470 these discrepancies are possibly due to a positive bias in the bottom-up emissions, mainly from the
471 anthropogenic sources, which have also been pointed out by Anderson et al. (2014) and Travis et
472 al. (2016). Larger OMI-model disagreement was found over the central/eastern US in June 2010
473 than in May, likely also due to the uncertainty in GEOS-Chem's soil or lightning NO_x emissions,
474 which appear to be high over these regions (Figure S1). The NO₂ columns in the GEOS-Chem
475 base simulation were overestimated in many northern China rural areas and underpredicted in a
476 few urban areas in the East Asia as well as a broad area in the southwestern China. The mismatches
477 between model and OMI NO₂ fell within the ranges of the comparison between the GOME2 NO₂
478 column product and six models' simulations over China in summer 2008 (Quennehen et al., 2016).
479 Also, the use of monthly-mean anthropogenic emissions as well as the overall rough treatment of
480 emission height and temporal profiles can be sources of uncertainty. These global model
481 evaluation results suggest that the EAS-NAM SR relationships analyzed using this inventory may
482 overall overestimate the NAM local contribution and underestimate the EAS contribution—Under
483 different chemical regimes, this statement would also rely on the quality of other O₃ precursors'
484 emissions in the HTAP2 inventory, and they may be associated with variable uncertainties
485 depending on the species or emission sector as introduced in Section 2.1. Therefore, careful
486 assessment of other key O₃ precursors' emissions in the inventory is needed in the future work. It
487 is important to note that uncertainty in satellite retrievals can prevent us from producing accurate
488 assessment on emissions (e.g., van Noije et al., 2006), and this comparison does not account for
489 the biases in the used OMI data, and would be further validated by using other OMI NO₂ products

490 as well as the bias-corrected (if applicable) in-situ NO₂ measurements. We also recommend more
491 global models to save their calculations more frequently, at least near the satellite overpassing
492 times, for a more comprehensive assessment of the emission inventory and a better understanding
493 of the model biases.

494 3.1.2. Evaluation of the global model O₃ performance in NAM and EAS

495
496 The monthly-mean surface O₃ from multiple global models' free runs was evaluated with
497 the CASTNET observations, at the stations with 95% of the hourly O₃ observation completeness
498 for the 1 May-30 June 2010 period. The mean biases and RMSEs for these two months were
499 summarized in Table 2a by US subregions. The three boundary condition-model as well as the
500 eight-model ensembles overall underpredicted O₃ in the western US (by ~3-6 ppbv), similar to the
501 HTAP1 model performance over these regions for May-June 2001 presented in Fiore et al. (2009).
502 This can be due to the underestimated trans-boundary pollution (as indicated by the evaluation of
503 modeled O₃ profiles with ozonesondes and satellite O₃ products). In addition, the coarser model
504 resolutions are less capable of resolving the local features that influence the pollutants' import
505 processes, chemical transformation, as well as regional processes such as the cross-state pollution
506 transport over complex terrains. The global RAQMS base simulation with satellite assimilation
507 improved the free tropospheric O₃ structure as its comparisons with the ozonesondes shows, which
508 also enhanced the simulated monthly-mean surface O₃ by up to >10 ppbv in the western US and
509 some coastal areas in the southeastern US (Figure S2, left). The global models overall significantly
510 overestimated O₃ in the other three subregions (by 8-12 ppbv), close to HTAP1 model performance
511 for May-June 2001 over the similar areas (Fiore et al., 2009) and in the Lapina et al. (2014) study
512 for 2010, in large part due to the uncertainties in the bottom-up emissions as discussed in Section
513 3.1.1. Satellite assimilation led to 2-6 ppbv higher RAQMS surface O₃ in the
514 central/southern/eastern US than in its free simulation, which are associated with higher positive
515 biases.
516

517
518 The surface O₃ performance by individual global models varies significantly, e.g., with the
519 RMSEs at all CASTNET sites ranging from ~9 ppbv to >15 ppbv (Table 2b). As reported in the
520 literature (e.g., Geddes et al., 2016; Travis et al., 2016), the representation of land use/land cover,
521 boundary layer mixing and chemistry can be sources of uncertainty for certain global model (i.e.,
522 GEOS-Chem), but how serious these issues were in the other models need to be investigated
523 further. Some other possible reasons include the variation of these models' non-anthropogenic
524 emission inputs and chemical mechanisms (Table 1c). Future work should emphasize on
525 evaluating and comparing all models on process level to better understand their performance.
526 Except in the northeastern US, the eight-model ensembles show better agreement with the
527 CASTNET O₃ observations than the three boundary condition-model ensemble. Overall the three-
528 model ensemble only outperforms one model but the eight-model ensemble outperforms seven
529 individuals. This reflects that averaging the results from a larger number of models in this case
530 more effectively cancelled out the positive or negative biases from the individual models.
531

532 The monthly-mean surface O₃ from multiple global models' free runs was also evaluated
533 with the EANET observations. Among the three boundary condition models, GEOS-Chem
534 produced higher O₃ than the other two throughout the year, and C-IFS O₃ is the lowest from April
535 to December. The three-model and eight-model ensembles are lower than the surface O₃

536 observations by <10 ppbv during high O₃ seasons (winter/spring), but show substantial (>10 ppbv)
537 positive biases during low O₃ seasons especially in July and August (Figure 3b), similar to the
538 HTAP1 model performance over Japan in 2001 (Fiore et al., 2009). During May-June 2010,
539 generally the models performed better at the Japanese sites than at the Korean sites (Table 2c),
540 with significant positive biases occurring at low O₃ regions (e.g., in central Japan) and negative
541 biases found at high O₃ regions, mainly owing to the uncertainty in the local and upwind emissions.
542 The different approaches to generate the monthly-mean modeled and the observed O₃ data may
543 have also contributed to these model-observation discrepancies. Overall O₃ performance by
544 individual models varies less significantly than at the CASTNET sites, with RMSEs ranging from
545 8.6 ppbv to ~13 ppbv (Table 2b). The three-model ensemble outperforms two individual models,
546 and the eight-model ensemble outperforms six individual models. Unlike at the CASTNET sites,
547 the three-model ensemble agrees better with the observations than the eight-model ensemble
548 (Table 2c).

549 3.1.3. Evaluation of the STEM regional base simulations w/ three sets of boundary conditions

550
551 The three STEM base simulations using different boundary conditions were evaluated with
552 the hourly O₃ observations at the CASTNET sites in the four US subregions. The evaluation
553 included the 8 May-30 June 2010 period to exclude the results during the one-week spin-up period.
554 The time series plots of observed and modeled O₃ at the western US CASTNET sites show that
555 STEM was capable of capturing several high O₃ periods, and it produced larger biases during the
556 nighttime (Figure 2c), as a result of the poorer WRF performance. Figure 2c and the evaluation
557 statistics in Table 3a-b indicate that STEM/C-IFS O₃ concentrations are associated with the highest
558 positive bias and RMSE, while the STEM/GEOS-Chem and STEM/RAQMS predictions were
559 positively and negatively biased by less than 2 ppbv, respectively, with similar RMSEs and
560 correlations with the observations. The quality of the three STEM simulation mean is closest to
561 the STEM/GEOS-Chem run, with the mean bias/RMSE of ~1.6/4.9 ppbv, much better than the
562 three-boundary model ensemble (-5.7/10.4 ppbv). However, this good performance can be a net
563 effect of incorrect partitioning between the trans-boundary and local source contributions, with the
564 former being underestimated and offsetting the overestimation of the latter. Switching the STEM
565 chemical boundary conditions to the assimilated RAQMS base simulation led to increases in the
566 simulated surface O₃ concentrations by >9 ppbv in the western US (Figure S2, right), associated
567 with higher positive biases (due to several factors discussed in the next paragraph). Regional-scale
568 assimilation could further reduce uncertainties introduced from regional meteorological and
569 emission inputs to obtain better modeled total O₃ and the partitioning of trans-boundary versus US
570 contributions (e.g., Huang et al., 2015).

571
572 The three STEM base simulations all significantly overpredicted O₃ over the rest of the US
573 in part due to the uncertainties in NO_x emissions, with the STEM/RAQMS associated with the
574 lowest RMSEs and mean biases, but STEM/C-IFS correlated best with the observations (Table
575 3b). These positive biases are higher than the global model ensembles', which can partially result
576 from the possible unrealistic VOC speciation of the emission inventory and the SAPRC 99
577 chemical mechanism: Although SAPRC mechanisms have been used in air quality modeling for
578 regulatory applications in some US states such as California, they usually produced higher O₃ than
579 other mechanisms such as the CB04 and the CB05 (which were used by some HTAP2 global
580 models, see Table 1c) over the US, and the comparisons between SAPRC 99 and SAPRC 2007
581

Deleted: overall overestimated

583 are still in progress (e.g., Luecken et al., 2008; Zhang et al., 2012; Cai et al., 2011). It is important
584 to timely update the chemical mechanisms in the chemistry models, and we also suggest to timely
585 upgrade the VOC speciation in the bottom-up emission inventories in the US to benefit the air
586 quality modeling. Additionally, the uncertainty from non-anthropogenic emissions, such as the
587 biogenic VOC emissions from WRF/MEGAN which is known to often have positive biases, can
588 be another cause: As Hogrefe et al. (2011) presented, the MEGAN emissions resulted in a higher
589 O₃ response to hypothetical anthropogenic NO_x emission reductions compared with another set of
590 biogenic emission input. Huang et al. (2017) showed that MEGAN's positive biases are in part
591 due to the positively-biased temperature and radiation in WRF, and reducing ~2°C in WRF's
592 temperature biases using a different land initialization approach led to ~20% decreases in
593 MEGAN's isoprene emission estimates in September 2013 over some southeastern US regions.
594 These temperature and radiation biases, can also be important sources of uncertainty in the
595 modeled O₃ production. Quantifying the impacts of overestimated biogenic emissions and the
596 biased weather fields that contributed to the biases in emissions on the modeled O₃ is still an
597 ongoing work. Some existing studies also reported O₃ and NO₂ biases from other regional models
598 in the eastern US, due to the chemical mechanism and biases in NO_x and biogenic VOC emissions
599 (e.g., Canty et al., 2015). We anticipate that the results from the Air Quality Model Evaluation
600 International Initiative (AQMEII) experiment (e.g., Schere et al., 2012; Solazzo et al., 2012;
601 Galmarini et al., 2015, 2017), which involves more regional model simulations over the US with
602 the similar set of boundary conditions but different chemical mechanisms and non-anthropogenic
603 emission inputs, can help better understand the causes of errors in the simulated total O₃.

604 3.2. *The NAM surface O₃ sensitivity to extra-regional anthropogenic pollutants*

606 3.2.1. Global model ensembles

607
608 The impact of all foreign (i.e. non-NAM) anthropogenic sources on NAM surface O₃ was
609 first explored, including the spatial distributions of the RERER metric (eq. (2)) based on various
610 global models' simulations (Figure 5), and the domain wide mean sensitivities R(O₃, non-NAM,
611 20%) (eq. (1d)) (Figure 6). Across the NAM, the strongest impacts were found in spring time
612 (March-April-May, larger than 1.5 ppbv in average over the domain) and the weakest impacts are
613 shown during the summertime (June-July-August, 1.0-1.3 ppbv), consistent with the existing
614 knowledge on the seasonal variability of the non-local pollution impacts on NAM for other years
615 (e.g., Fiore et al., 2009; Reidmiller et al., 2009). All global models indicate strong non-NAM
616 anthropogenic source impacts on the western US mainly due to the impact of its high elevation,
617 and also near the US-Mexico border areas, especially southern Texas, due to their vicinity to the
618 Mexican (not included in the NAM source regions, see Figure 1) emission sources. Over the
619 western states, stronger non-local impacts were reflected from the results based on higher-
620 horizontal resolution global models (e.g., the >0.6 RERER values from the half degree EMEP
621 model, corresponding to its higher R(O₃, non-NAM, 20%) values than the other models'), similar
622 to the findings in previous modeling studies (Lin et al., 2010, 2012a). Although on a coarse
623 horizontal resolution of 2.8°, OsloCTM3 suggests stronger extra-regional source influences on the
624 northwestern US and the US-Canada border regions than the other models. Its largest number of
625 vertical layers among all global models might be a cause. Larger-than-1 RERER values are often
626 seen near the urban areas and large point sources due to the titration, especially evident from the
627 higher resolution model results. The R(O₃, EAS, 20%) values are larger than 1/3 of the R(O₃, non-
628 NAM, 20%) (0.2-0.5 ppbv from April to June), more than 3-4 times higher than R(O₃, EUR, 20%)

629 and $R(O_3, SAS, 20\%)$. Note that all eight models contributed to the $R(O_3, EAS, 20\%)$ calculations,
630 but one or two models did not provide all necessary sensitivity runs to compute the RERER, $R(O_3,$
631 non-NAM, 20%), $R(O_3, EUR, 20\%)$, or $R(O_3, SAS, 20\%)$.

632
633 Comparing to the HTAP1 modeling results, the magnitudes of $R(O_3, EUR, 20\%)$ from this
634 study are smaller by a factor of 2-3; In contrast, the $R(O_3, non-NAM, 20\%)$ and $R(O_3, EAS, 20\%)$
635 values are >50% higher than the HTAP1 modeling results. The different HTAP1 and HTAP2
636 results are possibly due to the following three reasons: 1) the substantial improvement in the
637 European air quality over the past decades that is shown in Crippa et al. (2016) and Pouliot et al.
638 (2015), which contrasts with the growing anthropogenic emissions from the East Asia and other
639 developing countries during 2001-2010; 2) the changes in the HTAP2 experiment setup from
640 HTAP1. This includes the differences in the participating models, and the different region
641 definitions, e.g., EUR by HTAP1's definition includes regions in Russia/Belarusia/Ukraine,
642 Middle East and North Africa that are excluded from the HTAP2's EUR domain. For EAS and
643 SAS, however, the regions not overlapped by HTAP1 and HTAP2 are mostly in the less
644 populated/polluted regions; 3) the stronger trans-Pacific transport in 2010 than in 2000-2001, as
645 first introduced in Section 2.2.1. Interannual variability of $R(O_3, EAS, 20\%)$ and $R(O_3, non-NAM,$
646 20%) is also found between 2010 and 2008-2009, based on the SNU GEOS-Chem calculations
647 (Figure S3). Foreign anthropogenic pollution impact on NAM was stronger in 2010 than in 2008-
648 2009, especially in April-May. This can be in part due to the higher O_3 precursors' emissions in
649 2010 from extra-regions including the East Asia (Table S1), as well as the spring 2010
650 meteorological conditions that favored the trans-Pacific pollution transport.

651
652 These monthly- and regional-mean $R(O_3, EAS, 20\%)$ values suggest that despite dilution
653 along the great transport distance, the EAS anthropogenic sources still had distinguishable impact
654 on the NAM surface O_3 . Similar to the findings from the HTAP1 studies, the large intermodel
655 variability (as indicated in Table 4) in the estimates of intercontinental SR relationships indicates
656 the uncertainties of these models in representing the key atmospheric processes which needs more
657 investigations in the future. Figure 6b compares the $R(O_3, EAS, 20\%)$ estimated by individual
658 boundary condition models, their ensemble mean sensitivities, and the eight-global model mean.
659 The averaged $R(O_3, EAS, 20\%)$ from the boundary condition model results are smaller than the
660 eight-global model mean, and except for July-October 2010, GEOS-Chem gives higher $R(O_3, EAS,$
661 20%) than RAQMS and C-IFS, consistent with its highest O_3 prediction in the EAS source region
662 (Figure 3b). Overall, $R(O_3, EAS, 20\%)$ and its intermodel differences are much smaller than the
663 biases of the modeled total O_3 in NAM. Other factors can contribute more significantly to the
664 biases in the modeled total O_3 , such as the stratospheric O_3 intrusion and the local O_3 formation,
665 and assessing the impacts from these factors would be also helpful for understanding the
666 uncertainties in the modeled O_3 .

667
668 The O_3 sensitivities in response to the perturbations of individual species or sector
669 emissions in East Asia, estimated by the GEOS-Chem adjoint model, were also analyzed (Figure
670 S3). These sensitivities show similar seasonal variability to $R(O_3, EAS, 20\%)$, with the values
671 ~twice as high in the spring than in summer, also consistent with the results on previous years
672 based on the 20% emission perturbation approach (e.g., Fiore et al., 2009; Brown-Steiner and Hess,
673 2011; Emmons et al., 2012). However, this seasonal variability is weaker than the results based on
674 the tagged tracer approach for earlier years: Using the CAM-Chem model, Brown-Steiner and

Deleted: -than-normal

676 Hess (2011) reported that during the springtime, Asian O₃ created from the anthropogenic/biofuel
677 NO_x emissions affected NAM O₃ ~three times as strongly as in summer. This is because the
678 nonlinear O₃ chemistry, which is stronger outside of summer, caused larger O₃ responses to a 100%
679 reduction of NO_x emissions than 5 times of the O₃ responses to a 20% reduction of NO_x emissions.
680 The EAS anthropogenic NO_x emissions more strongly impacted the NAM surface O₃ than the
681 other major O₃ precursors, similar to the findings in Fiore et al. (2009) and Reidmiller et al. (2009)
682 using the perturbation approach, as well as the conclusions in Lapina et al. (2014) based on the
683 adjoint sensitivity analyses. Emissions from the power&industrial sectors are higher in East Asia
684 than the other sectors (Table S1), resulting in its stronger influences on the NAM surface O₃. As
685 the observed NO₂ columns started to drop since 2010 due to the effective denitration devices
686 implemented at the Chinese power and industrial plants (e.g., Liu et al., 2016), depending on the
687 changes in the VOC emissions, it is anticipated to see different R(O₃, EAS, 20%) values for the
688 years after 2010. Therefore, continued studies to assess the East Asian anthropogenic pollution
689 impacts on NAM during more recent years is needed. As emissions from various source sectors
690 can differ by their emitted altitudes and temporal (from diurnal to seasonal) profiles, efforts should
691 also be placed to have the models timely update the heights and temporal profiles of the emissions
692 from those various sectors.

694 3.2.2. Regional model sensitivities and their connections with the boundary condition models'

696 The monthly-mean STEM surface R(O₃, EAS, 20%) sensitivities based on different
697 boundary condition models were inter-compared, and also compared with the R(O₃, EAS, 20%)
698 estimated by their boundary condition models as well as the global model ensemble mean (Figure
699 7). For both May and June 2010, the domain-wide mean R(O₃, EAS, 20%) values from
700 STEM/RAQMS were higher than the estimates from RAQMS by 0.03 ppbv; the STEM/GEOS-
701 Chem R(O₃, EAS, 20%) values are lower than those of GEOS-Chem by 0.01-0.06 ppbv, and the
702 STEM/C-IFS R(O₃, EAS, 20%) is 0.02 ppbv higher than C-IFS's in June but slightly (<<0.01 ppbv)
703 lower in May. These differences are overall smaller than the inter-global model differences, and
704 can be due to various factors including the uncertainties in boundary condition chemical species
705 mapping, and the different meteorological/terrain fields/chemistry in the global and regional model
706 pairs. The STEM R(O₃, EAS, 20%) ensemble mean values, however, are less than 0.02 ppbv
707 different from its boundary condition model's ensemble mean for both months. The STEM R(O₃,
708 EAS, 20%) ensemble mean value in June is also close to the eight-global model ensemble mean,
709 but is ~0.05 ppbv lower than the eight-model mean in May. Choosing other/more global model
710 outputs as STEM's boundary conditions may lead to different STEM ensemble mean R(O₃, EAS,
711 20%) estimates. We also found that the period mean R(O₃, EAS, 20%) of ~0.2 ppbv sampled only
712 at the CASTNET sites (Table 3a) are smaller than those averaged in all model grids. This indicates
713 that currently the sparsely distributed surface network (especially over the western US that is more
714 strongly affected by the extra-regional sources than the other US regions) may miss many LRT
715 episodes that impact the NAM. The planned geostationary satellites with ~2-5 km footprint sizes
716 and hourly sampling frequency (Hilsenrath and Chance, 2013; Zoogman et al., 2017) will help
717 better capture the high O₃ and LRT episodes in these regions.

718
719 The spatial patterns of the monthly-mean STEM surface R(O₃, EAS, 20%) sensitivities
720 based on the three boundary condition models are notably different, but overall resemble what's
721 estimated by the corresponding boundary condition model, and the STEM sensitivities show more

722 local details in certain high elevation regions in the US west (Figure 8 shows the June 2010
723 conditions as an example). These different sensitivities were investigated further, by examining
724 the $R(O_3, EAS, 20\%)$ values near the source regions (i.e., East Asia) as well as near the receptor
725 regions (Figure 9). More East Asian anthropogenic O_3 seems to be transported at the upper
726 troposphere in RAQMS than in the other two models. GEOS-Chem and RAQMS $R(O_3, EAS, 20\%)$
727 sensitivities are similar over the EAS as well as the 500-900 hPa near the receptor in the eastern
728 Pacific (at $\sim 135^\circ W$), the altitudes US surface O_3 are most strongly sensitive to during the
729 summertime as concluded from previous studies (e.g., Huang et al., 2010, 2013a; Parrish et al.,
730 2010). Despite the close NAM domain-wide mean values from the STEM/GEOS-Chem and
731 STEM/RAQMS, the spatial patterns of $R(O_3, EAS, 20\%)$ over NAM differ in these two cases,
732 with the latter case showing sharper gradients especially in the western US, partially due to the
733 impact of its higher horizontal resolution. The $R(O_3, EAS, 20\%)$ values from STEM/C-IFS are
734 lower than from the other two cases both near the sources and at (near) NAM. The STEM surface
735 (also near surface, not shown in figures) $R(O_3, EAS, 20\%)$ does not spatially correlate well with
736 the column $R(O_3, EAS, 20\%)$, the latter of which contributed more to the base case O_3 columns,
737 indicating that a good portion of the transported East Asian pollution did not descend to the lower
738 altitudes to impact the boundary layer/ground level air quality. An additional regional simulation
739 was performed in which the STEM boundary conditions were downscaled from a RAQMS
740 simulation without the East Asian anthropogenic emissions. The non-linear emission perturbation-
741 O_3 response relationships, as the larger-than-1 S_{O_3} metric (eq. (3)) indicate, are seen across the
742 domain, for both the surface and column O_3 (Figure 8). S_{O_3} for column O_3 , ranging from 1.15-1.25
743 in most regions, are overall ~ 0.05 higher than S_{O_3} for the surface O_3 . Therefore, the full source
744 contribution obtained by linearly scaling the receptor regional mean O_3 sensitivity to the 20%
745 reduction in the source region emissions may be underestimated by at least $\sim 10\%$.

746 3.2.3. Regional model MDA8 sensitivities on all days and during the O_3 exceedances

748 The temporal variability of the STEM $R(O_3, EAS, 20\%)$ ensemble sensitivities were also
749 studied. For most US subregions, 3-6 LRT episodes (defined as when the sensitivities are above
750 the period mean) were identified during May-June. Only in certain regions, we find that the
751 planetary boundary layer heights (PBLHs) were higher during the LRT episodes (i.e., the daily
752 daytime-mean $R(O_3, EAS, 20\%)$ and PBLHs show medium/strong positive correlations ($r > 0.5$),
753 as these correlations may have been complicated by the relationships between the PBLHs and the
754 local influences. Throughout this period, the hourly $R(O_3, EAS, 20\%)$ and the observed O_3 at the
755 surface CASTNET sites are weakly correlated (Table 3a), but they display similar diurnal cycles
756 (e.g., Figures 2c and 2d for the western US sites), possibly because the deeper boundary layer
757 depth during the daytime enhanced entrainment down-mixing of the extra-regional pollutants to
758 the surface. The identified diurnal variability of the $R(O_3, EAS, 20\%)$ can cause differences in the
759 calculated MDA8 and all-hour mean $R(O_3, EAS, 20\%)$ values. Figure S4 shows that the mean
760 $R(MDA8, EAS, 20\%)$ values, usually at daytimes, are higher than the all-hour averaged $R(O_3,$
761 $EAS, 20\%)$ in most STEM model grids during both months. Therefore, it is important for more
762 HTAP2 participating models to save their outputs hourly in order to conveniently compute the
763 policy-relevant metrics for the O_3 sensitivities. Also, the hourly sampling frequency of the planned
764 geostationary satellites is anticipated to be more helpful for evaluating the impacts of the LRT
765 episodes.

Formatted: Font color: Text 1

Formatted: Font color: Text 1

767 The STEM R(MDA8, EAS, 20%) in all model grids within the four US subregions were
768 averaged on all days during May-June 2010 and only on the days when the simulated total MDA8
769 O₃ is over 70 ppbv (Figure 10). These sensitivities also show appreciable spatial variability: from
770 0.35-0.58 ppbv in the western US (also with the largest standard deviations, not shown), which is
771 slightly higher than the HTAP1 results reported by Reidmiller et al. (2009) for Spring 2001, to
772 ~0.1-0.25 ppbv in the rest three subregions, which is close to the Reidmiller et al. (2009) results.
773

774 Comparing the solid bar plots in Figures 10-11, we found that on all days in the three non-
775 western subregions, R(MDA8, EAS, 20%) values sampled at CASTNET sites are slightly smaller
776 than those computed for all model grids, while in the non-western states the opposite differences
777 are seen. This again suggests that expanding observation network would help better capture the
778 high O₃ and LRT episodes.
779

780 Figure 10 suggests smaller R(MDA8, EAS, 20%) values during the high O₃ days in all
781 subregions. However, STEM's total O₃ concentrations at CASTNET sites during the O₃
782 exceedances were substantially overpredicted in non-western US regions while significantly
783 underpredicted in the western US (see mean biases above the bar plots in Figure 11). Therefore,
784 the R(MDA8, EAS, 20%) values shown in Figure 10 during the model-based periods of O₃
785 exceedances can represent the sensitivities during the actual periods of O₃ compliance in non-
786 western US regions, and may not represent the sensitivities during all actual O₃ exceedances in the
787 western US. Figures 11-12 show that if calculated only at the CASTNET sites during the
788 exceedances, in non-western US regions, R(MDA8, EAS, 20%) is 0.02-0.07 ppbv smaller during
789 the high O₃ total days. This is qualitatively consistent with the findings in Reidmiller et al. (2009),
790 and is possibly because that the LRT impacts were stronger on some days with good dispersion
791 conditions when the NAAQS was not exceeded, but weaker on some high O₃ days under stagnant
792 conditions. In contrast, western US R(MDA8, EAS, 20%) at CASTNET sites was ~0.05 ppbv
793 higher on high O₃ days than for all days, and this differences are larger in rural/remote areas where
794 local influences are less dominant. As a result, the medium/strong positive correlations are found
795 between modeled LRT of pollution and the total O₃ in these regions (Table 3a; Lin et al., 2012a).
796

797 3.3. Case studies of spring (9 May) and summer (10 June) LRT events mixed with stratospheric 798 O₃ intrusions 799

800 Lin et al. (2012a, b) and Neuman et al. (2012) showed that the trans-Pacific pollution
801 transport intensely impacted the western US during 8-10 May, 2010, intermingled with a
802 stratospheric intrusion that contributed to at least 1/3 of the total O₃ in some high elevation regions.
803 This episode is indeed indicated by the O₃ and CO products from AIRS and TES at ~500 hPa over
804 the Eastern Pacific (Figure 13), and the observed TES and IASI O₃ profiles over the western US
805 indicated elevated O₃ levels (>80 ppbv) at 700-900 hPa. Huang et al. (2013b) found that the
806 meteorological conditions during this period (i.e., a strong jet at ~700 hPa with wind speed >20
807 m/s shifted southwesterly when passing the southern California and continued to travel towards
808 the mountain states), along with the orographic lifting, efficiently exported the southern California
809 anthropogenic pollution, which was chemically coupled with the extra-regional pollution and
810 significantly enhanced the O₃ levels in the US intermountain west.
811

Formatted: Font:8 pt, Not Superscript/ Subscript

Formatted: Font:8 pt

Deleted: actually

Deleted: non-exceedances in

Formatted: Font:8 pt, Not Superscript/ Subscript

Formatted: Font:8 pt

814 We selected this episode to compare the STEM surface total O₃ concentrations as well as
815 the R(O₃, EAS, 20%) sensitivities based on the different HTAP2 boundary condition models.
816 Figure 14 evaluates the simulated O₃ profiles in the western US from several STEM base
817 simulations against the TES and IASI O₃ retrievals, and Figures 15a-d indicate the performance of
818 the daily surface total MDA8 O₃ from these simulations. We found that the underestimated free
819 tropospheric O₃ from the STEM simulations that used any single free-running chemical boundary
820 conditions contributed to the underestimated STEM surface O₃ in the high elevation mountain
821 states: e.g., by 9-14 ppbv at three CASTNET sites (Grand Canyon National Park (NP), AZ;
822 Canyonlands NP, UT; and Rocky Mountain NP, CO) where O₃ exceedances were observed. The
823 unsatisfactory performance by free-running global models during high O₃ events would pose
824 difficulties for regional models (regardless of their resolutions and other configurations,
825 parameterization) to accurately estimate the SR relationships using boundary conditions
826 downscaled from these model runs. The STEM base simulation using the RAQMS assimilated
827 fields as the boundary conditions, agrees most with the observed O₃ at the CASTNET sites, as well
828 as the TES and IASI O₃ profiles in the western states. Similar to the conclusions drawn in Huang
829 et al. (2010, 2015) for summer 2008, we again demonstrated the robustness of satellite chemical
830 data assimilation for improving the boundary condition models' O₃ performance. As the
831 enhancement of O₃ due to the assimilation is much larger than the O₃ sensitivities to the EAS
832 anthropogenic emissions, the assimilation mainly improved the contributions from other sources,
833 possibly including the stratospheric O₃.

Deleted: such as

835 The quality of the model boundary conditions only indicates how well the total “transported
836 background” component is represented, and can not be directly connected with the accuracy of the
837 model estimated R(O₃, EAS, 20%) sensitivities, which also show notable intermodel differences:
838 The estimated R(MDA8, EAS, 20%) in the different STEM cases range from <1.0 ppbv to ~1.3
839 ppbv, at least 40% higher than the May-June period mean in Figures 10-11. The mean R(MDA8,
840 EAS, 20%) at three high O₃ CASTNET sites range from 0.73 (STEM/GEOS-Chem) to 0.98 ppbv
841 (STEM/C-IFS), with the mean S_{O₃} of ~1.14 at these sites based on the STEM/RAQMS runs due
842 to the nonlinear emission perturbation-O₃ response relationships (Figure 15e-h). The R(MDA8,
843 EAS, 100%) from the STEM/RAQMS case is as high as >7 ppbv over the high terrain regions.
844 These are of smaller magnitudes than the estimates in Lin et al. (2012a), possibly due to the
845 differences in the used models and the bottom-up emission inputs.

846
847 A stratospheric O₃ intrusion also affected the Northeast US on the same day, as revealed
848 by the satellite mid-tropospheric O₃ and CO observations (Figure 13). This intrusion was mixed
849 with LRT East Asian pollution (Figure 15 and Figure S5). However, this intrusion did not enhance
850 the NE boundary layer/surface O₃ concentrations, which were actually anomalously low
851 (MDA8<40 ppbv) as indicated by the model base simulations and the CASTNET observations
852 (Figure 15a-d). Similar characteristics during summertime stratospheric O₃ intrusion events
853 around this region have been discussed by Ott et al. (2016). The East Asian pollution less intensely
854 (<50%) affected the surface O₃ levels in these regions than in the US west, due to the greater
855 transport distances, stronger local emission influence on chemical production/loss, shallower
856 PBLHs, as well as the impact of the overall flat terrain in the US east.

Deleted: NE

Deleted: free

857
858 A summertime LRT event on 9-10 June is analyzed to contrast with the 9 May case study.
859 Lin et al. (2012b) showed that >80 ppbv of ozonesonde data in northern California at 2-6 km

863 measured the stratospheric O₃ remnants during this episode, and the transported stratospheric O₃
864 contributed to as much as ~50% of the total O₃ in southern California based on their model
865 calculations. We show that on 10 June over 100 ppbv of O₃, as well as <90 ppbv CO, was observed
866 by satellites at ~500 hPa above Nevada and northern California (Figure 16), which again was
867 substantially underestimated by all free-running models (Figure 17), resulting in the
868 underpredicted total O₃ at two CASTNET sites in southern California (Converse Station and
869 Joshua Tree NP) that experienced O₃ exceedances on this day (Figure 18a-c). The negative biases
870 in the “transported background” O₃ and surface MDA8 O₃ were successfully reduced by
871 incorporating satellite data (Figures 17 and 18d).

872
873 Figures 18e-h show that LRT of EAS anthropogenic pollution also strongly affected
874 southern California and Nevada. Notable intermodel differences are again found in the estimated
875 R(MDA8, EAS, 20%), but they are overall lower than on 9 May (<1.0 ppbv). The mean R(MDA8,
876 EAS, 20%) at the two high O₃ CASTNET sites range from 0.54 (STEM/C-IFS) to 0.86 ppbv
877 (STEM/RAQMS), with the mean S_{O₃} of ~1.13 at these sites based on the STEM/RAQMS runs
878 (Figure 18e-h). The R(MDA8, EAS, 100%) from the STEM/RAQMS case is as high as >6 ppbv
879 over southern California and Nevada. Compared to the spring event, R(MDA8, EAS, 20%) in the
880 eastern US are discernable only over a limited region, due to weaker transport and stronger local
881 chemical production/loss.

882 883 4. Conclusions and suggestions on future directions

884
885 In support of the HTAP Phase 2 experiment that involved high-resolution global models
886 and regional models’ participation to advance the understanding of the pollutants’ SR relationships
887 in the Northern Hemisphere, we conducted a number of regional scale STEM base and forward
888 sensitivity simulations over NAM during May-June 2010. STEM’s top and lateral chemical
889 boundary conditions were downscaled from three global models’ (i.e., GEOS-Chem, RAQMS,
890 and ECMWF C-IFS) base and sensitivity simulations (in which the East Asian anthropogenic
891 emissions were reduced by 20%). Despite dilution along the great transport distance, the East
892 Asian anthropogenic sources still had distinguishable impact on the NAM surface O₃, with the
893 period-mean NAM O₃ sensitivities to a 20% reduction of the East Asian anthropogenic emissions
894 (i.e., R(O₃, EAS, 20%)) ranging from ~0.24 ppbv (STEM/C-IFS) to ~0.34 ppbv (STEM/RAQMS).
895 The spatial patterns of the STEM surface O₃ sensitivities over NAM overall resembled those from
896 its corresponding boundary condition model, with regional/period mean R(O₃, EAS, 20%) differed
897 slightly (<10%) from its corresponding boundary condition model’s, which are smaller than those
898 among its boundary condition models. The boundary condition models’ two-month mean R(O₃,
899 EAS, 20%) was ~8% lower than the mean sensitivity estimated by eight global models. Therefore,
900 choosing other global model outputs as STEM’s boundary conditions may lead to different STEM
901 O₃ sensitivities. The biases and RMSEs in the simulated total O₃, which differed significantly
902 among models, can partially be due to the uncertainty in the bottom-up NO_x emission inputs
903 according to the model comparison with the OMI NO₂ columns, and future work on attributing the
904 intermodel differences on process level is particularly important for better understanding the
905 sources of uncertainties in the modeled total O₃ and its source contribution.

906
907 The HTAP2 multi-model ensemble mean R(O₃, EAS, 20%) values in 2010 were higher
908 than the HTAP1 reported 2001 conditions, due to a number of reasons including the impacts of

Deleted: multiple

910 the growing East Asian anthropogenic emissions, the interannual variability in atmospheric
911 circulation (i.e., stronger trans-Pacific transport in spring 2010 following an El Niño event), and
912 the different experiment designs of HTAP1 and HTAP2. The GEOS-Chem O₃ sensitivities in 2010
913 were also higher than the 2008-2009 conditions due to the increasing Asian emissions and the
914 spring 2010 meteorological conditions that favored the trans-Pacific pollution transport. The
915 GEOS-Chem sensitivity calculations indicate that the East Asian anthropogenic NO_x emissions
916 mattered more than the other East Asian O₃ precursors to the NAM O₃, qualitatively consistent
917 with previous adjoint sensitivity calculations. Continued research is needed on temporal changes
918 of emissions for different species and sectors in NAM and foreign countries as well as their impacts
919 on the SR relationships. As emissions from various source sectors can differ by emitted altitudes
920 and temporal profiles, efforts should also be placed to have the models timely update the height
921 and temporal profiles of the emissions from various sectors.

922
923 An additional STEM simulation was performed in which the boundary conditions were
924 downscaled from a RAQMS simulation without East Asian anthropogenic emissions (i.e., a 100%
925 emission reduction), to assess the scalability of the mean O₃ sensitivities to the size of the emission
926 perturbation. The scalability was found to be spatially varying, ranging from 1.15-1.25 for column
927 O₃ in most US regions, which were overall ~0.05 higher than the surface O₃'s. Therefore, the full
928 source contribution obtained by linearly scaling the NAM regional mean O₃ sensitivity to the 20%
929 reduction in the East Asian emissions may be underestimated by at least 10%. The underestimation
930 in other seasons of the HTAP2 study period may be higher and will need to be quantified in future
931 work. Also, motivated by Lapina et al. (2014), additional calculations will be conducted in future
932 to explore the scalability of different O₃ metrics in these cases. For future source attribution
933 analysis, in general it is recommended to directly choose the suitable size of the emission
934 perturbation based on the specific questions to address, and to avoid linearly scaling O₃
935 sensitivities that are based on other amounts of the perturbations.

936
937 The STEM O₃ sensitivities to the East Asian anthropogenic emissions (based on three
938 boundary condition models separately and averagely) were strong during 3-6 episodes in May-
939 June 2010, following similar diurnal cycles as the total O₃. Stronger East Asian anthropogenic
940 pollution impacts were estimated during the observed O₃ exceedances in the western US than on
941 all days, especially over the high terrain rural/remote areas; in contrast, the East Asian
942 anthropogenic pollution impacts were less strong during O₃ exceedances in other US regions. We
943 emphasized the importance of saving model results hourly for conveniently calculating policy-
944 relevant metrics, as well as the usefulness of hourly sampling frequency of the planned
945 geostationary satellites for better evaluating the impacts of the LRT events.

946
947 Based on model calculations, satellite O₃ (TES, JPL-IASI, and AIRS), CO (TES and AIRS)
948 and surface O₃ observations on 9 May 2010, we showed the different influences from stratospheric
949 O₃ intrusions along with the transported East Asian pollution on O₃ in the western and the eastern
950 US. This event was further compared with a summer event of 10 June 2010. During both events,
951 the unsatisfactory performance of free-running (i.e., without chemical data assimilation) global
952 models would pose difficulties for regional models (regardless of their resolutions and other
953 configurations, parameterization) to accurately simulate the surface O₃ and its source contribution
954 using boundary conditions downscaled from these model runs. Incorporating satellite (OMI and
955 MLS) O₃ data effectively improved the modeled O₃. As chemical data assimilation techniques

Deleted: -than-normal

Deleted: non-local

Deleted: continently calculate

Formatted: Font color: Text 1

Formatted: Font color: Text 1

959 keep developing (Bocquet et al., 2015), several HTAP2 participating global models have already
960 been able to assimilate single- or multi- constitute satellite atmospheric composition data (e.g.,
961 Miyazaki et al., 2012; Parrington et al., 2008, 2009; Huang et al., 2015; Inness et al., 2015;
962 Flemming et al., 2017). Comparing the performance of the assimilated fields from different models,
963 and making the global model assimilated chemical fields in the suitable format for being used as
964 boundary conditions would be very beneficial for future regional modeling, as well as for better
965 interpreting the pollutants' distributions especially during the exceptional events. Meanwhile,
966 efforts should also be devoted to advancing and applying higher-resolution regional scale
967 modeling and chemical data assimilation. Furthermore, although satellite observations have been
968 applied for improving the estimated US background O₃ (e.g., Huang et al., 2015), using satellite
969 (and/or other types of) observations to improve SR relationship studies also needs to be explored.
970 Some of the possible methods include: 1) The combination of data assimilation and the tagging
971 approach; 2) Introducing observation-constrained emission estimates in the emission perturbation
972 analyses.

974 **Acknowledgements**

975
976 The global and regional modeling results used in this study have been submitted to the
977 AeroCom database following the HTAP2 data submission guidelines ([http://iek8wikis.iek.fz-](http://iek8wikis.iek.fz-juelich.de/HTAPWiki/HTAP-2-data-submission)
978 [juelich.de/HTAPWiki/HTAP-2-data-submission](http://iek8wikis.iek.fz-juelich.de/HTAPWiki/HTAP-2-data-submission)), or can be made available upon request.
979 Technical support from Anna Carlin Benedictow, Brigitte Koffi, Jan Griesfeller, and Michael
980 Schulz regarding formatting and submitting the data to the AeroCom is acknowledged. MH thanks
981 the research resources at the University of Iowa and JPL/Caltech that supported this study, as well
982 as the travel funding from the US EPA for attending the related HTAP2 workshops. DKH and YD
983 recognize support from NASA AQASt. FD Acknowledges support from the Administrative
984 Arrangement. Part of this research was carried out at the Jet Propulsion Laboratory, California
985 Institute of Technology, under contract to the National Aeronautics and Space Administration.
986 Reference herein to any specific commercial product, process or service by trade name, trademark,
987 manufacturer or otherwise does not constitute or imply its endorsement by the United States
988 Government or the Jet Propulsion Laboratory, California Institute of Technology. The views,
989 opinions, and findings contained in this report are those of the author(s) and should not be
990 construed as an official National Oceanic and Atmospheric Administration or U.S. Government
991 position, policy, or decision. We also acknowledge the feedbacks from Dr. Gail Tonnesen, two
992 anonymous reviewers, and Dr. Meiyun Lin on earlier versions of this paper, that helped improve
993 its quality.

994 **References**

995
996
997 Anderson, D. C., Loughner, C. P., Diskin, G., Weinheimer, A., Canty, T., P., Salawitch, R. J.,
998 Worden, H. M., Fried, A., 25 Mikoviny, T., Wisthaler, A., and Dickerson, R., R. (2014),
999 Measured and modeled CO and NO_y in DISCOVER-AQ: An evaluation of emissions and
1000 chemistry over the eastern US, *Atmos. Environ.*, 96, 78-87, doi:
1001 10.1016/j.atmosenv.2014.07.004.

1002 Allen, D. J., Pickering, K. E., Pinder, R. W., Henderson, B. H., Appel, K. W., and Prados, A.
 1003 (2012), Impact of lightning-NO on eastern United States photochemistry during the summer
 1004 of 2006 as determined using the CMAQ model, *Atmos. Chem. Phys.*, 12, 1737-1758, doi:
 1005 10.5194/acp-12-1737-2012.
 1006 Ambrose, J.L., Reidmiller, D.R., and Jaffe, D.A. (2011), Causes of high O₃ in the lower free
 1007 troposphere over the Pacific Northwest as observed at the Mt. Bachelor Observatory. *Atmos.*
 1008 *Environ.*, 45, 5302–5315, doi: 10.1016/j.atmosenv.2011.06.056.
 1009 Anenberg, S. C., L. W. Horowitz, D. Q. Tong, and J. J. West (2010), An estimate of the global
 1010 burden of anthropogenic ozone and fine particulate matter on premature human mortality using
 1011 atmospheric modeling, *Environ. Health Perspect.*, 118(9), 1189–1195.
 1012 Avnery, S, D.L. Mauzerall, J. Liu, L.W. Horowitz (2011a), Global Crop Yield Reductions due to
 1013 Surface Ozone Exposure: 1. Year 2000 Crop Production Losses and Economic
 1014 Damage, *Atmos. Environ.*, 45, 2284-2296.
 1015 Avnery, S, D.L. Mauzerall, J. Liu, L.W. Horowitz (2011b), Global Crop Yield Reductions due to
 1016 Surface Ozone Exposure: 2. Year 2030 Potential Crop Production Losses and Economic
 1017 Damage under Two Scenarios of O₃ Pollution, *Atmos. Environ.*, 45, 2297-2309.
 1018 Beer, R., T. A. Glavich, and D. M. Rider (2001), Tropospheric emission spectrometer for the Earth
 1019 Observing System’s Aura satellite, *Applied Optics*, 40, 2356 – 2367.
 1020 Beer, R (2006), TES on the Aura Mission: Scientific Objectives, Measurements, and Analysis
 1021 Overview, *IEEE Transaction on Geoscience and Remote Sensing*, 44, 1102-1105.
 1022 Bian, J., A. Gettelman, H. Chen, and L. L. Pan (2007), Validation of satellite ozone profile
 1023 retrievals using Beijing ozonesonde data, *J. Geophys. Res.*, 112, D06305,
 1024 doi:10.1029/2006JD007502.
 1025 Bocquet, M., Elbern, H., Eskes, H., Hirtl, M., Žabkar, R., Carmichael, G. R., Flemming, J., Inness,
 1026 A., Pagowski, M., Pérez Camaño, J. L., Saide, P. E., San Jose, R., Sofiev, M., Vira, J.,
 1027 Baklanov, A., Carnevale, C., Grell, G., and Seigneur, C. (2015), Data assimilation in
 1028 atmospheric chemistry models: current status and future prospects for coupled chemistry
 1029 meteorology models, *Atmos. Chem. Phys.*, 15, 5325-5358, doi:10.5194/acp-15-5325-2015.
 1030 Boersma, K. F., Braak, R., van der A, R. J. (2011a), Dutch OMI NO₂ (DOMINO) data product
 1031 v2.0 HE5 data file user manual. http://www.temis.nl/docs/OMI_NO2_HE5_2.0_2011.pdf.
 1032 Boersma, K. F., Eskes, H. J., Dirksen, R. J., van der A, R. J., Veefkind, J. P., Stammes, P., Huijnen,
 1033 V., Kleipool, Q. L., Sneep, M., Claas, J., Leitão, J., Richter, A., Zhou, Y., Brunner, D. (2011b),
 1034 An improved tropospheric NO₂ column retrieval algorithm for the Ozone Monitoring
 1035 Instrument, *Atmos. Meas. Tech.*, 4, 1905-1928.
 1036 Bowman, K. W., Rodgers, C. D., Kulawik, S. S., Worden, J., Sarkissian, E., Osterman, G., Steck,
 1037 T., Lou, M., Eldering, A., Shephard, M., Worden, H., Lampel, M., Clough, S., Brown, P.,
 1038 Rinsland, C., Gunson, M., and Beer, R. (2006), Tropospheric Emission Spectrometer:
 1039 Retrieval method and error analysis, *IEEE Transaction on Geoscience and Remote Sensing*,
 1040 44 (5), 1297–1307, doi: 10.1109/TGRS.2006.871234.
 1041 Bowman, K., and D. K. Henze (2012), Attribution of direct ozone radiative forcing to spatially
 1042 resolved emissions, *Geophys. Res. Lett.*, 39, L22704, doi:10.1029/2012GL053274.

1043 Brioude, J., Angevine, W. M., Ahmadov, R., Kim, S.-W., Evan, S., McKeen, S. A., Hsie, E.-Y.,
1044 Frost, G. J., Neuman, J. A., Pollack, I. B., Peischl, J., Ryerson, T. B., Holloway, J., Brown, S.
1045 S., Nowak, J. B., Roberts, J. M., Wofsy, S. C., Santoni, G. W., Oda, T., and Trainer, M. (2013),
1046 Top-down estimate of surface flux in the Los Angeles Basin using a mesoscale inverse
1047 modeling technique: assessing anthropogenic emissions of CO, NO_x and CO₂ and their
1048 impacts, *Atmos. Chem. Phys.*, 13, 3661-3677, doi:10.5194/acp-13-3661-2013.
1049 Brown-Steiner, B., and P. Hess (2011), Asian influence on surface ozone in the United States: A
1050 comparison of chemistry, seasonality, and transport mechanisms, *J. Geophys. Res.*, 116,
1051 D17309, doi:10.1029/2011JD015846.
1052 Cai, C., J. T. Kelly, J. C. Avise, A. P. Kaduwela, and W. R. Stockwell (2011), Photochemical
1053 Modeling in California with Two Chemical Mechanisms: Model Intercomparison and
1054 Response to Emission Reductions, *J. Air & Waste Manage. Assoc.*, 61:5, 559-572, doi:
1055 10.3155/1047-3289.61.5.559.
1056 Canty, T. P., Hembeck, L., Vinciguerra, T. P., Anderson, D. C., Goldberg, D. L., Carpenter, S. F.,
1057 Allen, D. J., Loughner, C. P., Salawitch, R. J., and Dickerson, R. R. (2015), Ozone and NO_x
1058 chemistry in the eastern US: evaluation of CMAQ/CB05 with satellite (OMI) data, *Atmos.*
1059 *Chem. Phys.*, 15, 10965-10982, doi:10.5194/acp-15-10965-2015.
1060 Carmichael, G.R., Tang, Y., Kurata, G., Uno, I., Streets, D.G., Thongboonchoo, N., Woo, J.H.,
1061 Guttikunda, S., White, A., Wang, T., Blake, D.R., Atlas, E., Fried, A., Potter, B., Avery, M.A.,
1062 Sachse, G.W., Sandholm, S.T., Kondo, Y., Talbot, R.W., Bandy, A., Thornton, D., and Clarke,
1063 A.D. (2003a), Evaluating regional emission estimates using the TRACE-P observations, *J.*
1064 *Geophys. Res.*, 108 (D21), 8810, doi: 10.1029/2002JD003116.
1065 Carmichael, G.R., Tang, Y., Kurata, G., Uno, I., Streets, D., Woo, J.H., Huang, H., Yienger, J.,
1066 Lefer, B., Shetter, R., Blake, D., Atlas, E., Fried, A., Apel, E., Eisele, F., Cantrell, C., Avery,
1067 M., Barrick, J., Sachse, G., Brune, W., Sandholm, S., Kondo, Y., Singh, H., Talbot, R., Bandy,
1068 A., Thornton, D., Clarke, A., and Heikes, B. (2003b), Regional-scale chemical transport
1069 modeling in support of the analysis of observations obtained during the TRACE-P experiment,
1070 *J. Geophys. Res.*, 108 (D21), 8823, doi: 10.1029/2002JD003117.
1071 Carter, W. P. L. (2000), Documentation of the SAPRC-99 chemical mechanism for VOC
1072 Reactivity Assessment, final report to California Air Resources Board, Contract No. 92-329
1073 and 95-308.
1074 Cooper, O. R., et al. (2010), Increasing springtime ozone mixing ratios in the free troposphere over
1075 western North America, *Nature*, 463, doi: 10.1038/nature08708.
1076 Cooper, O. R., Oltmans, S. J., Johnson, B. J., Brioude, J., Angevine, W., Trainer, M., Parrish, D.
1077 D., Ryerson, T. R., Pollack, I., Cullis, P. D., Ives, M. A., Tarasick, D. W., Al-Saadi, J., and
1078 Stajner, I. (2011), Measurement of western U.S. baseline ozone from the surface to the
1079 tropopause and assessment of downwind impact regions, *J. Geophys. Res.*, 116, D00V03, doi:
1080 10.1029/2011JD016095.
1081 Cooper, O., et al. (2016), Western NA Performance Evaluation for HTAP2, HTAP2 workshop,
1082 Potsdam, Germany, 2016.
1083 Crippa, M., Janssens-Maenhout, G., Dentener, F., Guizzardi, D., Sindelarova, K., Muntean, M.,
1084 Van Dingenen, R., and Granier, C. (2016), Forty years of improvements in European air
1085 quality: regional policy-industry interactions with global impacts, *Atmos. Chem. Phys.*, 16,
1086 3825-3841, doi:10.5194/acp-16-3825-2016.

Formatted: Subscript

1087 Emmons, L. K., Hess, P. G., Lamarque, J.-F., and Pfister, G. G. (2012), Tagged ozone mechanism
1088 for MOZART-4, CAM-chem and other chemical transport models, *Geosci. Model Dev.*, 5,
1089 1531-1542, doi:10.5194/gmd-5-1531-2012.

1090 Eskes, H. J. and Boersma, K. F. (2003), Averaging kernels for DOAS total-column satellite
1091 retrievals, *Atmos. Chem. Phys.*, 3, 1285-1291.

1092 Fiore, A. M., et al. (2009), Multimodel estimates of intercontinental source receptor relationships
1093 for ozone pollution, *J. Geophys. Res.*, 114, D04301, doi:10.1029/2008JD010816.

1094 Fiore, A. M., J. T. Oberman, M. Y. Lin, L. Zhang, O. E. Clifton, D. J. Jacob, V. Naik, L. W.
1095 Horowitz, J. P. Pinto, and G. P. Milly (2014), Estimating North American background ozone
1096 in U.S. surface air with two independent global models: Variability, uncertainties, and
1097 recommendations, *Atmos. Environ.*, 96, 284–300, doi: 10.1016/j.atmosenv.2014.07.045.

1098 Flemming, J., Huijnen, V., Arteta, J., Bechtold, P., Beljaars, A., Blechschmidt, A.-M., Diamantakis,
1099 M., Engelen, R. J., Gaudel, A., Inness, A., Jones, L., Josse, B., Katragkou, E., Marecal, V.,
1100 Peuch, V.-H., Richter, A., Schultz, M. G., Stein, O., and Tsikerdekis, A. (2015), Tropospheric
1101 chemistry in the Integrated Forecasting System of ECMWF, *Geosci. Model Dev.*, 8, 975-1003,
1102 doi:10.5194/gmd-8-975-2015.

1103 Flemming, J., Benedetti, A., Inness, A., Engelen, R., Jones, L., Huijnen, V., Remy, S., Parrington,
1104 M., Suttie, M., Bozzo, A., Peuch, V.-H., Akritidis, D., and Katragkou, E. (2017), The CAMS
1105 interim Reanalysis of Carbon Monoxide, Ozone and Aerosol for 2003–2015, *Atmos. Chem.*
1106 *Phys.*, 17, 1945-1983, doi:10.5194/acp-17-1945-2017.

1107 Galmarini, S., C. Hogrefe, D. Brunner, P. Makar, A. Baklanov (2015), Preface to the AQMEII p2
1108 Special issue, *Atmos. Environ.*, 115, 340-344.

1109 Galmarini, S., Koffi, B., Solazzo, E., Keating, T., Hogrefe, C., Schulz, M., Benedictow, A.,
1110 Griesfeller, J. J., Janssens-Maenhout, G., Carmichael, G., Fu, J., and Dentener, F. (2017),
1111 Technical note: Coordination and harmonization of the multi-scale, multi-model activities
1112 HTAP2, AQMEII3, and MICS-Asia3: simulations, emission inventories, boundary conditions,
1113 and model output formats, *Atmos. Chem. Phys.*, 17, 1543-1555, doi:10.5194/acp-17-1543-
1114 2017.

1115 Geddes, J. A., Heald, C. L., Silva, S. J., and Martin, R. V. (2016), Land cover change impacts on
1116 atmospheric chemistry: simulating projected large-scale tree mortality in the United States,
1117 *Atmos. Chem. Phys.*, 16, 2323-2340, doi:10.5194/acp-16-2323-2016.

1118 Gery, M. W., G. Z. Whitten, J. P. Killus, and M. C. Dodge (1989), A photochemical kinetics
1119 mechanism for urban and regional scale computer modeling, *J. Geophys. Res.*, 94, 12,925 –
1120 12,956, doi:10.1029/JD094iD10p12925.

1121 Granier, C., Lamarque, J. F., Mieville, A., Muller, J. F., Olivier, J., Orlando, J., Peters, J., Petron,
1122 G., Tyndall, G., and Wallens, S. (2005), POET, a database of surface emissions of ozone
1123 precursors, <http://www.aero.jussieu.fr/projet/ACCENT/POET.php>.

1124 Gratz, L.E., Jaffe, D.A., and Hee, J.R. (2014), Causes of increasing ozone and decreasing carbon
1125 monoxide in springtime at the Mt. Bachelor Observatory from 2004 to 2013, *Atmos. Environ.*,
1126 109, 323–330, doi: 10.1016/j.atmosenv.2014.05.076.

1127 Guenther, A. B., X. Jiang, C. L. Heald, T. Sakulyanontvittaya, T. Duhl, L. K. Emmons, and X.
1128 Wang (2012), The Model of Emissions of Gases and Aerosols from Nature version 2.1
1129 (MEGAN2.1): an extended and updated framework for modeling biogenic emissions, *Geosci.*
1130 *Model Dev.*, 5 (6), 1471-1492.

1131 Henze, D. K., Hakami, A., and Seinfeld, J. H. (2007), Development of the adjoint of GEOS-Chem,
1132 *Atmos. Chem. Phys.*, 7, 2413–2433, doi:10.5194/acp-7-2413-2007.

1133 Hilsenrath, E., and K. Chance (2013), NASA ups the TEMPO on monitoring air pollution, *Earth*
 1134 *Obs.*, 25, 10–15.
 1135 Hogrefe, C., Isukapalli, S., Tang, X., Georgopoulos, P., He, S., Zalewsky, E., Hao, W., Ku, J.,
 1136 Key, T., and Sistla, G. (2011), Impact of biogenic emission uncertainties on the simulated
 1137 response of ozone and fine Particulate Matter to anthropogenic emission reductions, *J. Air*
 1138 *Waste Manage.*, 61, 92–108.
 1139 Huang, M., Carmichael, G. R., Adhikary, B., Spak, S. N., Kulkarni, S., Cheng, Y. F., Wei, C.,
 1140 Tang, Y., Parrish, D. D., Oltmans, S. J., D'Allura, A., Kaduwela, A., Cai, C.,
 1141 Weinheimer, A. J., Wong, M., Pierce, R. B., Al-Saadi, J. A., Streets, D. G., and Zhang, Q.
 1142 (2010), Impacts of transported background ozone on California air quality during the
 1143 ARCTAS-CARB period – a multi-scale modeling study, *Atmos. Chem. Phys.*, 10, 6947-6968,
 1144 doi: 10.5194/acp-10-6947-2010.
 1145 Huang, M., Carmichael, G. R., Chai, T., Pierce, R. B., Oltmans, S. J., Jaffe, D. A.,
 1146 Bowman, K. W., Kaduwela, A., Cai, C., Spak, S. N., Weinheimer, A. J., Huey, L. G., and
 1147 Diskin, G. S. (2013a), Impacts of transported background pollutants on summertime western
 1148 US air quality: model evaluation, sensitivity analysis and data assimilation, *Atmos. Chem.*
 1149 *Phys.*, 13, 359-391, doi: 10.5194/acp-13-359-2013.
 1150 Huang, M., Bowman, K. W., Carmichael, G. R., Pierce, R. B., Worden, H. M., Luo, M., Cooper,
 1151 O. R., Pollack, I. B., Ryerson, T. B., Brown, S. S. (2013b), Impact of southern California
 1152 anthropogenic emissions on ozone pollution in the mountain states, *J. Geophys. Res.*, 118,
 1153 12784-12803, doi: 10.1002/2013JD020205.
 1154 Huang, M., et al. (2014), Changes in nitrogen oxides emissions in California during 2005–2010
 1155 indicated from top-down and bottom-up emission estimates, *J. Geophys. Res.*, 119, 12,928–
 1156 12,952, doi: 10.1002/2014JD022268, 2014.
 1157 Huang, M., et al. (2015), Improved Western US Background Ozone Estimates via Constraining
 1158 Nonlocal and Local Source Contributions using Aura TES and OMI Observations, *J. Geophys.*
 1159 *Res.*, 120, 3572–3592, doi: 10.1002/2014JD022993.
 1160 Huang, M., Carmichael, G. R., Crawford, J. H., Wisthaler, A., Zhan, X., Hain, C. R., Lee, P., and
 1161 Guenther, A. B. (2017), Linkages between land initialization of the NASA-Unified WRF v7
 1162 and biogenic isoprene emission estimates during the SEAC4RS and DISCOVER-AQ airborne
 1163 campaigns, *Geosci. Model Dev. Discuss.*, doi:10.5194/gmd-2017-13, in review.
 1164 Inness, A., Blechschmidt, A.-M., Bouarar, I., Chabrillat, S., Crepulja, M., Engelen, R. J., Eskes,
 1165 H., Flemming, J., Gaudel, A., Hendrick, F., Huijnen, V., Jones, L., Kapsomenakis, J.,
 1166 Katragkou, E., Keppens, A., Langerock, B., de Mazière, M., Melas, D., Parrington, M., Peuch,
 1167 V. H., Razinger, M., Richter, A., Schultz, M. G., Suttie, M., Thouret, V., Vrekoussis, M.,
 1168 Wagner, A., and Zerefos, C. (2015), Data assimilation of satellite-retrieved ozone, carbon
 1169 monoxide and nitrogen dioxide with ECMWF's Composition-IFS, *Atmos. Chem. Phys.*, 15,
 1170 5275-5303, doi:10.5194/acp-15-5275-2015.
 1171 Jaffe, D.A. (2011), Relationship between surface and free tropospheric ozone in the Western U.S.,
 1172 *Environ. Sci. Technol.*, 45, 432–438, doi: 10.1021/es1028102.
 1173 Janssens-Maenhout, G., Crippa, M., Guizzardi, D., Dentener, F., Muntean, M., Pouliot, G.,
 1174 Keating, T., Zhang, Q., Kurokawa, J., Wankmüller, R., Denier van der Gon, H., Kuenen, J. J.
 1175 P., Klimont, Z., Frost, G., Darras, S., Koffi, B., and Li, M. (2015), HTAP_v2.2: a mosaic of
 1176 regional and global emission grid maps for 2008 and 2010 to study hemispheric transport of
 1177 air pollution, *Atmos. Chem. Phys.*, 15, 11411-11432, doi:10.5194/acp-15-11411-2015.

1178 Jacob, D. J., Logan, J. A., and Murti, P. P. (1999), Effect of rising Asian emissions on surface
1179 ozone in the United States, *Geophys. Res. Lett.*, 26, 2175-2178, doi: 10.1029/1999GL900450.
1180 Jerret, M., R. T. Burnett, C. A. Popo, III, K. Ito, G. Thurston, D. Krewski, Y. Shi, E. Calle, and M.
1181 Thun (2009), Long-Term Ozone Exposure and Mortality, the New England Journal of
1182 Medicine, 360, 1085-1096, doi: 10.1056/NEJMoa0803894.
1183 Kaiser, J. W., Heil, A., Andreae, M. O., Benedetti, A., Chubarova, N., Jones, L., Morcrette, J.-J.,
1184 Razinger, M., Schultz, M. G., Suttie, M., and van der Werf, G. R. (2012), Biomass burning
1185 emissions estimated with a global fire assimilation system based on observed fire radiative
1186 power, *Biogeosciences*, 9, 527-554, doi:10.5194/bg-9-527-2012.
1187 Kalnay, E., and Co-authors (1996), The NCEP/NCAR 40-Year Reanalysis Project, *Bulletin of the*
1188 *American Meteorological Society*, 77, 437-471.
1189 Kim, S.-W., B. C. McDonald, S. Baidar, S. S. Brown, B. Dube, R. A. Ferrare, G. J. Frost, R. A.
1190 Harley, J. S. Holloway, H.-J. Lee, et al. (2016), Modeling the weekly cycle of NO_x and CO
1191 emissions and their impacts on O₃ in the Los Angeles-South Coast Air Basin during the CalNex
1192 2010 field campaign, *J. Geophys. Res. Atmos.*, 121, 1340-1360, doi:10.1002/2015JD024292.
1193 Koffi, B., Dentener, F., Janssens-Maenhout, G., Guizzardi, D., Crippa, M., Diehl, T., Galmarini,
1194 S., and Solazzo, E.: Hemispheric Transport Air Pollution (HTAP): Specification of the HTAP2
1195 experiments – Ensuring harmonized modelling, EUR 28255 EN – Scientific and Technical
1196 Research Reports, doi:10.2788/725244, 2016.
1197 Langford, A. O., Brioude, J., Cooper, O.R., Senff, C.J., Alvarez II, R.J., Hardesty, R.M., Johnson,
1198 B.J., and Oltmans, S.J. (2011), Stratospheric influence on surface ozone in the Los Angeles
1199 area during late spring and early summer of 2010, *J. Geophys. Res. Atmos.*, 117, D00V06, doi:
1200 10.1029/2011JD016766.
1201 Lapina, K., D. K. Henze, J. B. Milford, M. Huang, M. Lin, A. M. Fiore, G. Carmichael, G. G.
1202 Pfister, and K. Bowman (2014), Assessment of source contributions to seasonal vegetative
1203 exposure to ozone in the U.S., *J. Geophys. Res. Atmos.*, 119, 324-340,
1204 doi:10.1002/2013JD020905.
1205 Levelt, P.F., E. Hilsenrath, G.W. Leppelmeier, G.H.J. van den Oord, P.K. Bhartia, J. Tamminen,
1206 J.F. de Haan and J.P. Veefkind (2006), Science Objectives of the Ozone Monitoring Instrument,
1207 *IEEE Transaction on Geoscience and Remote Sensing*, 44, 1199-1208.
1208 Li, M., Zhang, Q., Kurokawa, J.-I., Woo, J.-H., He, K., Lu, Z., Ohara, T., Song, Y., Streets, D. G.,
1209 Carmichael, G. R., Cheng, Y., Hong, C., Huo, H., Jiang, X., Kang, S., Liu, F., Su, H., and
1210 Zheng, B. (2017), MIX: a mosaic Asian anthropogenic emission inventory under the
1211 international collaboration framework of the MICS-Asia and HTAP, *Atmos. Chem. Phys.*, 17,
1212 935-963, doi:10.5194/acp-17-935-2017.
1213 Lin, M., Holloway, T., Carmichael, G. R., and Fiore, A. M. (2010), Quantifying pollution inflow
1214 and outflow over East Asia in spring with regional and global models, *Atmos. Chem. Phys.*,
1215 10, 4221-4239, doi:10.5194/acp-10-4221-2010.
1216 Lin, M., A. M. Fiore, L. W. Horowitz, O. R. Cooper, V. Naik, J. Holloway, B. J. Johnson, A.
1217 Middlebrook, S. J. Oltmans, I. B. Pollack, T. B. Ryerson, J. X. Warner, C. Wiedinmyer, J.
1218 Wilson, B. Wyman (2012a), Transport of Asian ozone pollution into surface air over the
1219 western United States in spring, *J. Geophys. Res.*, 117, D00V07, doi: 10.1029/2011JD016961.
1220 Lin, M., A. Fiore, O. R. R. Cooper, L. W. Horowitz, A. O. O. Langford, H. Levy II, B. J. Johnson,
1221 V. Naik, S. J. Oltmans, and C. J. Senff (2012b), Springtime high surface ozone events over the
1222 western United States: Quantifying the role of stratospheric intrusions, *J. Geophys. Res.*, 117,
1223 D00V22, doi: 10.1029/2012JD018151.

1224 Lin, M., L.W. Horowitz, S. J. Oltmans, A. M. Fiore, S. Fan (2014), Tropospheric ozone trends at
1225 Manna Loa Observatory tied to decadal climate variability, *Nature Geoscience*, 7, 136-143,
1226 doi:10.1038/NGEO2066.

1227 Lin, M., L. W. Horowitz, O. R. Cooper, D. Tarasick, S. Conley, L. T. Iraci, B. Johnson, T. Leblanc,
1228 I. Petropavlovskikh, and E. L. Yates (2015), Revisiting the evidence of increasing springtime
1229 ozone mixing ratios in the free troposphere over western North America, *Geophys. Res. Lett.*,
1230 42, 8719–8728, doi:10.1002/2015GL065311.

1231 Lin, M., Horowitz, L. W., Payton, R., Fiore, A. M., and Tonnesen, G. (2016), US surface ozone
1232 trends and extremes from 1980–2014: Quantifying the roles of rising Asian emissions,
1233 domestic controls, wildfires, and climate, *Atmos. Chem. Phys. Discuss.*, doi:10.5194/acp-
1234 2016-1093, in review.

1235 Liu, F., Q. Zhang, R. J. van der A, B. Zheng, D. Tong, L. Yan, Y. Zheng, and K. He (2016), Recent
1236 reduction in NO_x emissions over China: Synthesis of satellite observations and emission
1237 inventories, *Environ. Res. Lett.*, 11 (11), 114002, doi: 10.1088/1748-9326/11/11/114002.

1238 Livesey, N.J., M.J. Filipiak, L. Froidevaux, W.G. Read, A. Lambert, M.L. Santee, J.H. Jiang, H.C.
1239 Pumphrey, J.W. Waters, R.E. Cofield, D.T. Cuddy, W.H. Daffer, B.J. Drouin, R.A. Fuller, R.F.
1240 Jarnot, Y.B. Jiang, B.W. Knosp, Q.B. Li, V.S. Perun, M.J. Schwartz, W.V. Snyder, P.C. Stek,
1241 R.P. Thurstans, P.A. Wagner, M. Avery, E.V. Browell, J-P. Cammas, L.E. Christensen, G.S.
1242 Diskin, R-S. Gao, H-J. Jost, M. Loewenstein, J.D. Lopez, P. Nedelec, G.B. Osterman, G.W.
1243 Sachse, and C.R. Webster (2008), Validation of Aura Microwave Limb Sounder O₃ and CO
1244 observations in the upper troposphere and lower stratosphere, *J. Geophys. Res.* 113, D15S02,
1245 doi:10.1029/2007JD008805.

1246 Luecken, D.J., S. Phillips, G. Sarwar, C. Jang, Effects of using the CB05 vs. SAPRC99 vs. CB4
1247 chemical mechanism on model predictions (2008), Ozone and gas-phase photochemical
1248 precursor concentrations, *Atmos. Environ.*, 42 (23), 5805-5820, doi:
1249 10.1016/j.atmosenv.2007.08.056.

1250 Maas, R. and P. Grennfelt (eds) (2016), Towards Cleaner Air Scientific Assessment Report 2016.
1251 EMEP Steering Body and Working Group on Effects of the Convention on Long-Range
1252 Transboundary Air Pollution, Oslo,
1253 http://www.unece.org/fileadmin/DAM/env/lrtap/ExecutiveBody/35th_session/CLRTAP_Scientific_Assessment_Report_-_Final_20-5-2016.pdf.

1254 Madronich, S., Flocke, S., Zeng, J., Petropavlovskikh, I., and Lee-Taylor, J. (2002), The
1255 Tropospheric Ultra-violet Visible (TUV) model Manual,
1256 [https://www2.acom.ucar.edu/modeling/tropospheric-ultraviolet-and-visible-tuv-radiation-](https://www2.acom.ucar.edu/modeling/tropospheric-ultraviolet-and-visible-tuv-radiation-model)
1257 [model](https://www2.acom.ucar.edu/modeling/tropospheric-ultraviolet-and-visible-tuv-radiation-model).

1258 Mauzerall, D. L. and Wang, X. (2001), Protecting Agricultural Crops from the Effects of
1259 Tropospheric Ozone Exposure: Reconciling Science and Standard Setting in the United States,
1260 Europe and Asia, *Annual Review of Energy and the Environment*, 26, 237-268.

1261 McDonald-Buller, E. C., et al. (2011), Establishing policy relevant background (PRB) ozone
1262 concentrations in the United States, *Environ. Sci. Technol.*, 45, 9484–9497.

1264 Meijer, E. W., van Velthoven, P. F. J., Brunner, D. W., Huntrieser, H., and Kelder, H. (2001),
1265 Improvement and evaluation of the parameterization of nitrogen oxide production by lightning,
1266 *Phys. Chem. Earth Pt. C*, 26, 577–583.

1267 Mesinger, F., DiMego, G., Kalnay, E., Mitchell, K., Shafran, P. C., Ebisuzaki, W., Jovic, D.,
 1268 Woollen, J., Rogers, E., Berbery, E. H., Ek, M. B., Fan, Y., Grumbine, R., Higgins, W., Li, H.,
 1269 Lin, Y., Manikin, G., Parrish, D. and Shi, W. (2006), North American Regional Reanalysis,
 1270 Bulletin of the American Meteorological Society, 87(3), 343–360, doi: 10.1175/BAMS-87-3-
 1271 343.
 1272 Miyazaki, K., Eskes, H. J., Sudo, K., Takigawa, M., van Weele, M., Boersma, K. F. (2012),
 1273 Simultaneous assimilation of satellite NO₂, O₃, CO, and HNO₃ data for the analysis of
 1274 tropospheric chemical composition and emissions, *Atmos. Chem. Phys.*, 12, 9545-9579.
 1275 Monks, P. S., Archibald, A. T., Colette, A., Cooper, O., Coyle, M., Derwent, R., Fowler, D.,
 1276 Granier, C., Law, K. S., Mills, G. E., Stevenson, D. S., Tarasova, O., Thouret, V., von
 1277 Schneidemesser, E., Sommariva, R., Wild, O., and Williams, M. L. (2015), Tropospheric
 1278 ozone and its precursors from the urban to the global scale from air quality to short-lived
 1279 climate forcer, *Atmos. Chem. Phys.*, 15, 8889-8973, doi:10.5194/acp-15-8889-2015.
 1280 Murray, L. T., D. J. Jacob, J. A. Logan, R. C. Hudman, and W. J. Koshak (2012), Optimized
 1281 regional and interannual variability of lightning in a global chemical transport model
 1282 constrained by LIS/OTD satellite data, *J. Geophys. Res.*, 117, D20307,
 1283 doi:10.1029/2012JD017934.
 1284 National Research Council (NRC) (2009), global sources of local pollution-An Assessment of
 1285 Long-Range Transport of Key Air Pollutants to and from the United States, 35-66,
 1286 http://books.nap.edu/openbook.php?record_id=12743&page=35.
 1287 Neuman, J. A., et al. (2012), Observations of ozone transport from the free troposphere to the Los
 1288 Angeles basin, *J. Geophys. Res. Atmos.*, 117, D00V09, doi: 10.1029/2011JD016919.
 1289 Oetjen, H., Payne, V. H., Kulawik, S. S., Eldering, A., Worden, J., Edwards, D. P., Francis, G. L.,
 1290 Worden, H. M., Clerbaux, C., Hadji-Lazarou, J., and Hurtmans, D. (2014), Extending the
 1291 satellite data record of tropospheric ozone profiles from Aura-TES to MetOp-IASI:
 1292 characterisation of optimal estimation retrievals, *Atmos. Meas. Tech.*, 7, 4223–4236,
 1293 doi:10.5194/amt-7-4223-2014.
 1294 Oetjen, H., Payne, V. H., Neu, J. L., Kulawik, S. S., Edwards, D. P., Eldering, A., Worden, H. M.,
 1295 and Worden, J. R. (2016), A joint data record of tropospheric ozone from Aura-TES and
 1296 MetOp-IASI, *Atmos. Chem. Phys.*, 16, 10229-10239, doi:10.5194/acp-16-10229-2016.
 1297 Ott, L. E., B. N. Duncan, A. M. Thompson, G. Diskin, Z. Fasnacht, A. O. Langford, M. Lin, A. M.
 1298 Molod, J. E. Nielsen, S. E. Pusede, et al. (2016), Frequency and impact of summertime
 1299 stratospheric intrusions over Maryland during DISCOVER-AQ (2011): New evidence from
 1300 NASA's GEOS-5 simulations, *J. Geophys. Res. Atmos.*, 121, 3687–3706,
 1301 doi:10.1002/2015JD024052.
 1302 Park, R. J., D. J. Jacob, B. D. Field, R. M. Yantosca, and M. Chin (2004), Natural and
 1303 transboundary pollution influences on sulfate-nitrate-ammonium aerosols in the United States:
 1304 Implications for policy, *J. Geophys. Res.*, 109, D15204, doi:10.1029/2003JD004473.
 1305 Parrington, M., D. B. A. Jones, K. W. Bowman, L. W. Horowitz, A. M. Thompson, D. W. Tarasick,
 1306 and J. C. Witte (2008), Estimating the summertime tropospheric ozone distribution over North
 1307 America through assimilation of observations from the Tropospheric Emission Spectrometer,
 1308 *J. Geophys. Res.*, 113, D18307, doi:10.1029/2007JD009341.
 1309 Parrington, M., D. B. A. Jones, K. W. Bowman, A. M. Thompson, D. W. Tarasick, J. Merrill, S.
 1310 J. Oltmans, T. Leblanc, J. C. Witte, and D. B. Millet (2009), Impact of the assimilation of
 1311 ozone from the Tropospheric Emission Spectrometer on surface ozone across North America,
 1312 *Geophys. Res. Lett.*, 36, L04802, doi:10.1029/2008GL036935.

1313 Parrish, D. D., D. B. Millet, and A. H. Goldstein (2009), Increasing ozone in marine boundary
1314 layer inflow at the west coasts of North America and Europe, *Atmos. Chem. Phys.*, 9, 1303–
1315 1323, doi:10.5194/acp-9-1303-2009.

1316 Parrish, D. D., Aikin, K. C., Oltmans, S. J., Johnson, B. J., Ives, M., and Sweeny, C. (2010), Impact
1317 of transported background ozone inflow on summertime air quality in a California ozone
1318 exceedance area, *Atmos. Chem. Phys.*, 10, 10093-10109, doi:10.5194/acp-10-10093-2010.

1319 Parrish, D. D., et al. (2012), Long-term changes in lower tropospheric baseline ozone
1320 concentrations at northern mid-latitudes, *Atmos. Chem. Phys.*, 12, 11,485–11,504,
1321 doi:10.5194/acp-12-11485-2012.

1322 Pierce, R. B., et al. (2007), Chemical data assimilation estimates of continental U.S. ozone and
1323 nitrogen budgets during the Intercontinental Chemical Transport Experiment–North America,
1324 *J. Geophys. Res.*, 112, D12S21, doi:10.1029/2006JD007722.

1325 Pierce, R. B., et al. (2009), Impacts of background ozone production on Houston and Dallas, Texas,
1326 air quality during the Second Texas Air Quality Study field mission, *J. Geophys. Res.*, 114,
1327 D00F09, doi:10.1029/2008JD011337.

1328 Pouliot, G., H. A.C. Denier van der Gon, J. Kuenen, J. Zhang, M. D. Moran, P.A. Makar (2015),
1329 Analysis of the emission inventories and model-ready emission datasets of Europe and North
1330 America for phase 2 of the AQMEII project, *Atmos. Environ.*, 115, 345-360.

1331 Qu, Z., D. K. Henze, S. L. Capps, Y. Wang, X. Xu, J. Wang (2016), Monthly top-down NO_x
1332 emissions for China (2005-2012): a hybrid inversion method and trend analysis, submitted.

1333 Quennehen, B., Raut, J.-C., Law, K. S., Daskalakis, N., Ancellet, G., Clerbaux, C., Kim, S.-W.,
1334 Lund, M. T., Myhre, G., Olivié, D. J. L., Safieddine, S., Skeie, R. B., Thomas, J. L., Tsyro, S.,
1335 Bazureau, A., Bellouin, N., Hu, M., Kanakidou, M., Klimont, Z., Kupiainen, K.,
1336 Myriokefalitakis, S., Quaas, J., Rumbold, S. T., Schulz, M., Cherian, R., Shimizu, A., Wang,
1337 J., Yoon, S.-C., and Zhu, T. (2016), Multi-model evaluation of short-lived pollutant
1338 distributions over east Asia during summer 2008, *Atmos. Chem. Phys.*, 16, 10765-10792,
1339 doi:10.5194/acp-16-10765-2016.

1340 Reidmiller, D. R., Fiore, A. M., Jaffe, D. A., Bergmann, D., Cuvelier, C., Dentener, F. J., Duncan,
1341 B. N., Folberth, G., Gauss, M., Gong, S., Hess, P., Jonson, J. E., Keating, T., Lupu, A., Marmar,
1342 E., Park, R., Schultz, M. G., Shindell, D. T., Szopa, S., Vivanco, M. G., Wild, O., and Zuber,
1343 A. (2009), The influence of foreign vs. North American emissions on surface ozone in the US,
1344 *Atmos. Chem. Phys.*, 9, 5027-5042, doi:10.5194/acp-9-5027-2009.

1345 Rodgers, C. D. (2000), *Inverse Methods for Atmospheric Sounding: Theory and Practice*, World
1346 Sci., Singapore.

1347 Ryerson, T. B., Andrews, A. E., Angevine, W. M., Bates, T. S., Brock, C. A., Cairns, B., Cohen,
1348 R. C., Cooper, O. R., de Gouw, J. A., Fehsenfeld, F. C., Ferrare, R. A., Fischer, M. L., Flagan,
1349 R. C., Goldstein, A. H., Hair, J. W., Hardesty, R. M., Hostetter, C. A., Jimenez, J. L., Langford,
1350 A. O., McCauley, E., McKeen, S. A., Molina, L. T., Nenes, A., Oltmans, S. J., Parrish, D. D.,
1351 Pederson, J. R., Pierce, R. B., Prather, K., Quinn, P. K., Seinfeld, J. H., Senff, C. J., Sorooshian,
1352 A., Stutz, J., Surratt, J. D., Trainer, M., Volkamer, R., Williams, E. J., Wofsy, S. C. (2013),
1353 The 2010 California Research at the Nexus of Air Quality and Climate Change (CalNex) field
1354 study, *J. Geophys. Res.*, 118, 5830–5866.

1355 Schere, K. J. Flemming, R. Vautard, C. Chemel, A. Colette, C. Hogrefe, B. Bessagnet, F. Meleux,
1356 R. Mathur, S. Roselle, R.-M. Hu, R. S. Sokhi, S. T. Rao, S. Galmarini (2012), Trace gas/aerosol
1357 boundary concentrations and their impacts on continental-scale AQMEII modeling domains,
1358 *Atmos. Environ.*, 53, 38-50, doi: 10.1016/j.atmosenv.2011.09.043.

1359 Shindell, D. T., G. Faluvegi, D. M. Koch, G. A. Schmidt, N. Unger, and S. E. Bauer (2009),
 1360 Improved attribution of climate forcing to emissions, *Science*, 326, 716–718, doi:
 1361 10.1126/science.1174760.
 1362 Shindell, D. T., et al. (2013), Radiative forcing in the ACCMIP historical and future climate
 1363 simulations, *Atmos. Chem. Phys.*, 13, 2939–2974, doi:10.5194/acp-13-2939-2013.
 1364 Simpson, D., Benedictow, A., Berge, H., Bergström, R., Emberson, L. D., Fagerli, H., Flechard,
 1365 C. R., Hayman, G. D., Gauss, M., Jonson, J. E., Jenkin, M. E., Nyiri, A., Richter, C., Semeena,
 1366 V. S., Tsyro, S., Tuovinen, J.-P., Valdebenito, Á., and Wind, P. (2012), The EMEP MSC-W
 1367 chemical transport model – technical description, *Atmos. Chem. Phys.*, 12, 7825–7865,
 1368 doi:10.5194/acp-12-7825-2012.
 1369 Sindelarova, K., Granier, C., Bouarar, I., Guenther, A., Tilmes, S., Stavrakou, T., Müller, J.-F.,
 1370 Kuhn, U., Stefani, P., and Knorr, W. (2014), Global data set of biogenic VOC emissions
 1371 calculated by the MEGAN model over the last 30 years, *Atmos. Chem. Phys.*, 14, 9317–9341,
 1372 doi:10.5194/acp-14-9317-2014.
 1373 Skamarock, W. C., J. B. Klemp, J. Dudhia, D. Gill, D. M. Barker, W. Wang, and J. G. Powers
 1374 (2008), A description of the Advanced Research WRF version 3 (Available at
 1375 www.mmm.ucar.edu/wrf/users/docs/arwv3.pdf).
 1376 Smith, K. R., Jerrett, M., and Anderson, H. R. et al. (2009), Public health benefits of strategies to
 1377 reduce greenhouse-gas emissions: health implications of short-lived greenhouse pollutants,
 1378 *Lancet*, doi: 10.1016/S0140-6736 (09) 61716-5.
 1379 Solazzo, E. R. Bianconi, R. Vautard, K. W. Appel, M. D. Moran, C. Hogrefe, B. Bessagnet, J.
 1380 Brandt, J. H. Christensen, C. Chemel, I. Coll, H. D. van der Gon, J. Ferreira, R. Forkel, X. V.
 1381 Francis, G. Grell, P. Grossi, A. B. Hansen, A. Jeričević, L. Kraljević, A. I. Miranda, U.
 1382 Nopmongkol, G. Pirovano, M. Prank, A. Riccio, K. N. Sartelet, M. Schaap, J. D. Silver, R. S.
 1383 Sokhi, J. Vira, J. Werhahn, R. Wolke, G. Yarwood, J. Zhang, S.T. Rao, S. Galmarini (2012),
 1384 Model evaluation and ensemble modelling of surface-level ozone in Europe and North
 1385 America in the context of AQMEII, *Atmos. Environ.*, 53, 60-74, , doi:
 1386 10.1016/j.atmosenv.2012.01.003.
 1387 Søvde, O. A., Prather, M. J., Isaksen, I. S. A., Berntsen, T. K., Stordal, F., Zhu, X., Holmes, C. D.,
 1388 and Hsu, J. (2012), The chemical transport model Oslo CTM3, *Geosci. Model Dev.*, 5, 1441–
 1389 1469, doi:10.5194/gmd-5-1441-2012.
 1390 Sudo, K., M. Takahashi, J. Kurokawa, and H. Akimoto (2002), Chaser: A global chemical model
 1391 of the troposphere, 1. Model description, *J. Geophys. Res.*, 107(D17), 4339,
 1392 doi:10.1029/2001JD001113.
 1393 Stevenson, D. S., et al. (2006), Multimodel ensemble simulations of present-day and near-future
 1394 tropospheric ozone, *J. Geophys. Res.*, 111, D08301, doi:10.1029/2005JD006338.
 1395 Stevenson, D. S., et al. (2013), Tropospheric ozone changes, radiative forcing and attribution to
 1396 emissions in the Atmospheric Chemistry and Climate Model Intercomparison Project
 1397 (ACCMIP), *Atmos. Chem. Phys.*, 13, 3063–3085, doi:10.5194/acp-13-3063-2013.
 1398 Susaya, J., Kim, K.-H., Shon, Z.-H., Brown R. J. (2013), Demonstration of long-term increases in
 1399 tropospheric O₃ levels: Causes and potential impacts, *Chemosphere*, 92, 1520–1528.
 1400 Task Force on Hemispheric Transport of Air Pollution (HTAP) (2010), 2010 Final Assessment
 1401 report, Part A: Ozone and particulate matter,
 1402 [http://www.htap.org/activities/2010_Final_Report/HTAP%202010%20Part%20A%2011040](http://www.htap.org/activities/2010_Final_Report/HTAP%202010%20Part%20A%20110407.pdf)
 1403 [7.pdf](http://www.htap.org/activities/2010_Final_Report/HTAP%202010%20Part%20A%20110407.pdf).

1404 Tilmes, S., Lamarque, J.-F., Emmons, L. K., Kinnison, D. E., Marsh, D., Garcia, R. R., Smith, A.
 1405 K., Neely, R. R., Conley, A., Vitt, F., Val Martin, M., Tanimoto, H., Simpson, I., Blake, D. R.,
 1406 and Blake, N. (2016), Representation of the Community Earth System Model (CESM1)
 1407 CAM4-chem within the Chemistry- Climate Model Initiative (CCMI), *Geosci. Model Dev.*, 9,
 1408 1853– 1890, doi:10.5194/gmd-9-1853-2016.
 1409 Travis, K. R., Jacob, D. J., Fisher, J. A., Kim, P. S., Marais, E. A., Zhu, L., Yu, K., Miller, C. C.,
 1410 Yantosca, R. M., Sulprizio, M. P., Thompson, A. M., Wennberg, P. O., Crouse, J. D., St.
 1411 Clair, J. M., Cohen, R. C., Laughner, J. L., Dibb, J. E., Hall, S. R., Ullmann, K., Wolfe, G. M.,
 1412 Pollack, I. B., Peischl, J., Neuman, J. A., and Zhou, X. (2016), Why do models overestimate
 1413 surface ozone in the Southeast United States?, *Atmos. Chem. Phys.*, 16, 13561-13577,
 1414 doi:10.5194/acp-16-13561-2016.
 1415 United Nations Environment Programme and World Meteorological Organization (2011),
 1416 Integrated Assessment of Black Carbon and Tropospheric Ozone: Summary for Decision
 1417 Makers, http://www.unep.org/dewa/Portals/67/pdf/Black_Carbon.pdf.
 1418 US EPA (2016a), Implementation of the 2015 Primary Ozone NAAQS: Issues Associated with
 1419 Background Ozone White Paper for Discussion,
 1420 <https://www.epa.gov/sites/production/files/2016-03/documents/whitepaper-bgo3-final.pdf>.
 1421 US EPA (2016b), High level summary of background ozone workshop,
 1422 [https://www.epa.gov/sites/production/files/2016-03/documents/bgo3-high-level-](https://www.epa.gov/sites/production/files/2016-03/documents/bgo3-high-level-summary.pdf)
 1423 [summary.pdf](https://www.epa.gov/sites/production/files/2016-03/documents/bgo3-high-level-summary.pdf).
 1424 van der Werf, G. R., Randerson, J. T., Giglio, L., Collatz, G. J., Mu, M., Kasibhatla, P. S., Morton,
 1425 D. C., DeFries, R. S., Jin, Y., and van Leeuwen, T. T. (2010), Global fire emissions and the
 1426 contribution of deforestation, savanna, forest, agricultural, and peat fires (1997–2009), *Atmos.*
 1427 *Chem. Phys.*, 10, 11707-11735, doi:10.5194/acp-10-11707-2010.
 1428 van Noije, T. P. C., Eskes, H. J., Dentener, F. J., Stevenson, D. S., Ellingsen, K., Schultz, M. G.,
 1429 Wild, O., Amann, M., Atherton, C. S., Bergmann, D. J., Bey, I., Boersma, K. F., Butler, T.,
 1430 Cofala, J., Drevet, J., Fiore, A. M., Gauss, M., Hauglustaine, D. A., Horowitz, L. W., Isaksen,
 1431 I. S. A., Krol, M. C., Lamarque, J.-F., Lawrence, M. G., Martin, R. V., Montanaro, V., Müller,
 1432 J.-F., Pitari, G., Prather, M. J., Pyle, J. A., Richter, A., Rodriguez, J. M., Savage, N. H., Strahan,
 1433 S. E., Sudo, K., Szopa, S., and van Roozendaal, M. (2006), Multi-model ensemble simulations
 1434 of tropospheric NO₂ compared with GOME retrievals for the year 2000, *Atmos. Chem. Phys.*,
 1435 6, 2943-2979, doi:10.5194/acp-6-2943-2006.
 1436 Verstraeten, W. W., K. F. Boersma, J. Zörner, M. A. F. Allaart, K. W. Bowman, and J. R. Worden
 1437 (2013), Validation of six years of TES tropospheric ozone retrievals with ozonesonde
 1438 measurements: Implications for spatial patterns and temporal stability in the bias, *Atmos. Meas.*
 1439 *Tech.*, 6, 1413–1423.
 1440 Verstraeten, W. W., J. L. Neu, J. E. Williams, K. W. Bowman, J. R. Worden, and K. F. Boersma
 1441 (2015), Rapid increases in tropospheric ozone production and export from China, *Nature*
 1442 *Geoscience*, 8, 690–695, doi:10.1038/ngeo2493.
 1443 Wang, H., D. J. Jacob, P. L. Sager, D. G. Streets, R. J. Park, A. B. Gilliland, and A. van Donkelaar
 1444 (2009), Surface ozone background in the United States: Canadian and Mexican pollution
 1445 influences, *Atmos. Environ.*, 43(6), 1310–1319, doi:10.1016/j.atmosenv.2008.11.036.
 1446 Wang, Y., Konopka, P., Liu, Y., Chen, H., Müller, R., Plöger, F., Riese, M., Cai, Z., and Lü, D.
 1447 (2012), Tropospheric ozone trend over Beijing from 2002–2010: ozonesonde measurements
 1448 and modeling analysis, *Atmos. Chem. Phys.*, 12, 8389-8399, doi:10.5194/acp-12-8389-2012.

1449 Warneke, C., J. A. deGouw, J. S. Holloway, J. Peischl, T. B. Ryerson, E. Atlas, D. Blake, M.
1450 Trainer, and D. D. Parrish (2012), Multiyear trends in volatile organic compounds in Los
1451 Angeles, California: Five decades of decreasing emissions, *J. Geophys. Res.*, 117, D00V17,
1452 doi:10.1029/2012JD017899.

1453 Warner, J. X., McCourt Comer, M., Barnet, C. D., McMillan, W. W., Wolf, W., Maddy, E., and
1454 Sachse, G. (2007), A comparison of satellite tropospheric carbon monoxide measurements
1455 from AIRS and MOPITT during INTEX-A, *J. Geophys. Res.*, 112, D12S17,
1456 doi:10.1029/2006JD007925, 2007.

1457 Wiedinmyer, C., Akagi, S. K., Yokelson, R. J., Emmons, L. K., Al-Saadi, J. A., Orlando, J. J., and
1458 Soja, A. J. (2011), The Fire INventory from NCAR (FINN): a high resolution global model to
1459 estimate the emissions from open burning, *Geosci. Model Dev.*, 4, 625-641, doi:10.5194/gmd-
1460 4-625-2011.

1461 Wigder, N.L., Jaffe, D.A., Herron-Thorpe, F.L., and Vaughan, J.K. (2013), Influence of daily
1462 variations in baseline ozone on urban air quality in the United States Pacific Northwest, *J.*
1463 *Geophys. Res.*, 118, 3343–3354, doi: 10.1029/2012JD018738.

1464 Wild, O., Fiore, A. M., Shindell, D. T., Doherty, R. M., Collins, W. J., Dentener, F. J., Schultz, M.
1465 G., Gong, S., MacKenzie, I. A., Zeng, G., Hess, P., Duncan, B. N., Bergmann, D. J., Szopa,
1466 S., Jonson, J. E., Keating, T. J., and Zuber, A. (2012), Modelling future changes in surface
1467 ozone: a parameterized approach, *Atmos. Chem. Phys.*, 12, 2037-2054, doi:10.5194/acp-12-
1468 2037-2012.

1469 Wu, S., B. N. Duncan, D. J. Jacob, A. M. Fiore, and O. Wild (2009), Chemical nonlinearities in
1470 relating intercontinental ozone pollution to anthropogenic emissions, *Geophys. Res. Lett.*, 36,
1471 L05806, doi:10.1029/2008GL036607.

1472 Yarwood, G., Rao, S., Yocke, M., and Whitten, G. (2005), Updates to the carbon bond chemical
1473 mechanism: CB05. Final report to the US EPA, EPA Report Number: RT-0400675.

1474 Zhang, L., Jacob, D. J., Boersma, K. F., Jaffe, D. A., Olson, J. R., Bowman, K. W., Worden, J. R.,
1475 Thompson, A. M., Avery, M. A., Cohen, R. C., Dibb, J. E., Flock, F. M., Fuelberg, H. E.,
1476 Huey, L. G., McMillan, W. W., Singh, H. B., and Weinheimer, A. J. (2008), Transpacific
1477 transport of ozone pollution and the effect of recent Asian emission increases on air quality in
1478 North America: an integrated analysis using satellite, aircraft, ozonesonde, and surface
1479 observations, *Atmos. Chem. Phys.*, 8, 6117-6136, doi:10.5194/acp-8-6117-2008.

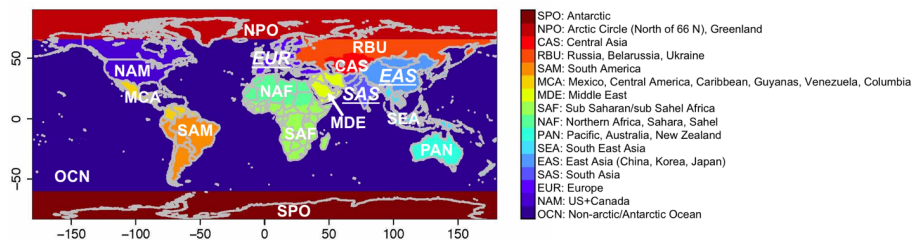
1480 Zhang, L., Jacob, D. J., Kopacz, M., Henze, D. K., Singh, K., and Jaffe, D. A. (2009),
1481 Intercontinental source attribution of ozone pollution at western U.S. sites using an adjoint
1482 method, *Geophys. Res. Lett.*, 36, L11810, doi: 10.1029/2009GL037950.

1483 Zhang, L., D. J. Jacob, N. V. Downey, D. A. Wood, D. Blewitt, C. C. Carouge, A. van Donkelaar,
1484 D. B. A. Jones, L. T. Murray, and Y. Wang (2011), Improved estimate of the policy-relevant
1485 background ozone in the United States using the GEOS-Chem global model with 1/2°×2/3°
1486 horizontal resolution over North America, *Atmos. Environ.*, 45, 6769–6776, doi:
1487 10.1016/j.atmosenv.2011.07.054.

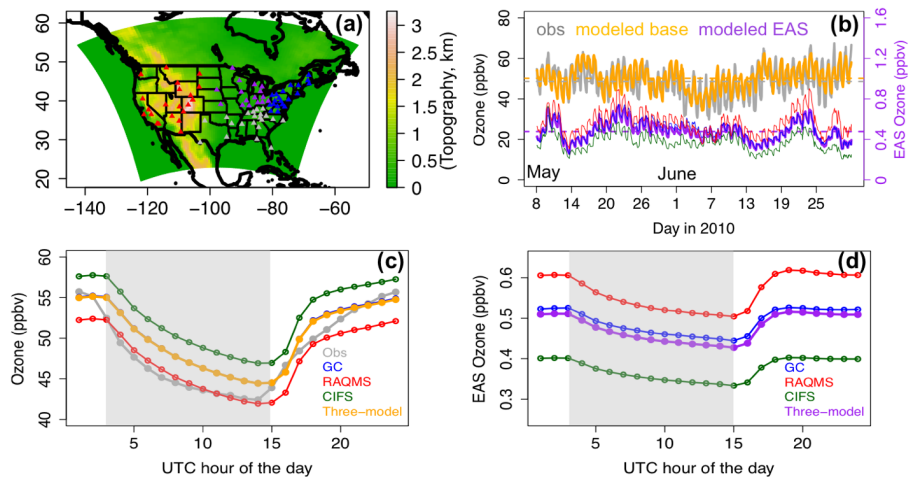
1488 Zhang, Q., Yuan, B., Shao, M., Wang, X., Lu, S., Lu, K., Wang, M., Chen, L., Chang, C.-C., and
1489 Liu, S. C. (2014), Variations of ground-level O₃ and its precursors in Beijing in summertime
1490 between 2005 and 2011, *Atmos. Chem. Phys.*, 14, 6089-6101, doi:10.5194/acp-14-6089-2014.

1491 Zhang, Y., Y. Chen, G. Sarwar, and K. Schere (2012), Impact of gas-phase mechanisms on
1492 Weather Research Forecasting Model with Chemistry (WRF/Chem) predictions: Mechanism
1493 implementation and comparative evaluation, *J. Geophys. Res.*, 117, D01301,
1494 doi:10.1029/2011JD015775.

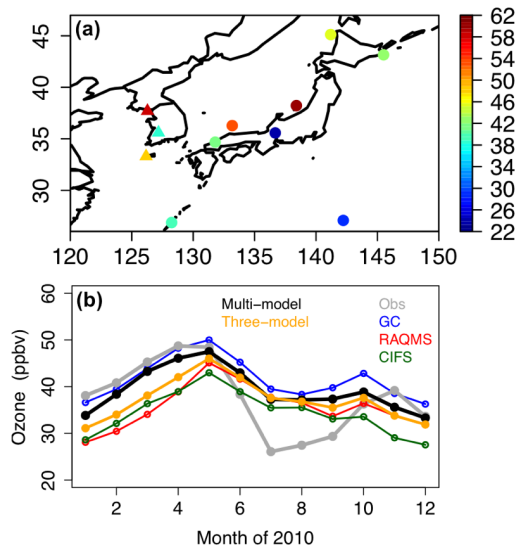
1495 [Zoogman, P., X. Liu, R.M. Suleiman, W.F. Pennington, D.E. Flittner, J.A. Al-Saadi, B.B. Hilton,](#)
1496 [D.K. Nicks, M.J. Newchurch, J.L. Carr, S.J. Janz, M.R. Andraschko, A. Arola, B.D. Baker,](#)
1497 [B.P. Canova, C. Chan Miller, R.C. Cohen, J.E. Davis, M.E. Dussault, D.P. Edwards, J.](#)
1498 [Fishman, A. Ghulam, G. González Abad, M. Grutter, J.R. Herman, J. Houck, D.J. Jacob, J.](#)
1499 [Joiner, B.J. Kerridge, J. Kim, N.A. Krotkov, L. Lamsal, C. Li, A. Lindfors, R.V. Martin, C.T.](#)
1500 [McElroy, C. McLinden, V. Natraj, D.O. Neil, C.R. Nowlan, E.J. O'Sullivan, P.I. Palmer, R.B.](#)
1501 [Pierce, M.R. Pippin, A. Saiz-Lopez, R.J.D. Spurr, J.J. Szykman, O. Torres, J.P. Veefkind, B.](#)
1502 [Veihelmann, H. Wang, J. Wang, and K. Chance \(2017\), Tropospheric emissions: Monitoring](#)
1503 [of pollution \(TEMPO\), Journal of Quantitative Spectroscopy and Radiative Transfer, 186, 17-](#)
1504 [39, doi: 10.1016/j.jqsrt.2016.05.008.](#)



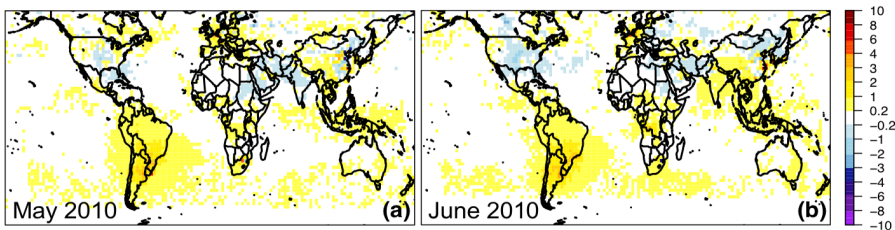
1505
 1506 **Figure 1.** Definitions of the 16 source regions used in HTAP2 SR relationship study (More details
 1507 in Koffi et al., 2016). The map is plotted based on data on a $0.1^\circ \times 0.1^\circ$ resolution grid. We focus
 1508 in this study on the impact of anthropogenic pollution from selected non-North American source
 1509 regions (i.e., EAS, SAS, and EUR), whose names are underlined and in italic.
 1510



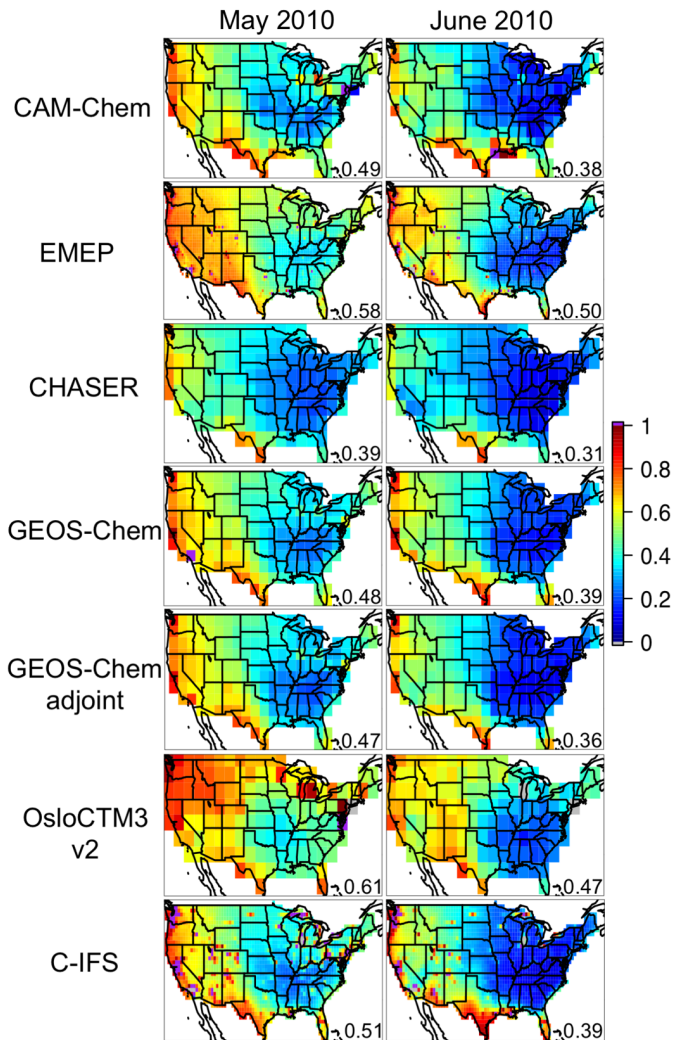
1511
 1512 **Figure 2.** (a) The 60 km STEM NAM domain, colored by the model topography. The CASTNET
 1513 sites used in the STEM base O_3 evaluation are marked as triangles in different colors that identify
 1514 the subregions they belong to (red: western US; grey: southern US; purple: Midwest; blue:
 1515 northeastern US). (b) Evaluation of the STEM modeled (averaged from the three base simulations
 1516 using the GEOS-Chem, ECMWF C-IFS, and RAQMS base runs as the chemical boundary
 1517 conditions) hourly O_3 at the western US (i.e., EPA regions 8, 9, and 10) CASTNET sites.
 1518 Observations, modeled base O_3 and the modeled $R(O_3, EAS, 20\%)$ are in grey, orange, and purple
 1519 lines, respectively. The horizontal dashed lines indicate the period mean values. The $R(O_3, EAS,$
 1520 $20\%)$ values from STEM calculations using three different chemical boundary conditions are
 1521 shown separately in thin lines (blue: GEOS-Chem; red: RAQMS; green: C-IFS). The period-mean
 1522 diurnal variability of the STEM modeled (c) base and (d) $R(O_3, EAS, 20\%)$ at the western US
 1523 CASTNET sites. The STEM calculations using three different chemical boundary conditions are
 1524 shown separately as well as averagely. Light grey-shaded areas indicate the local standard
 1525 nighttime (from 6/7 pm to 7/8 am).



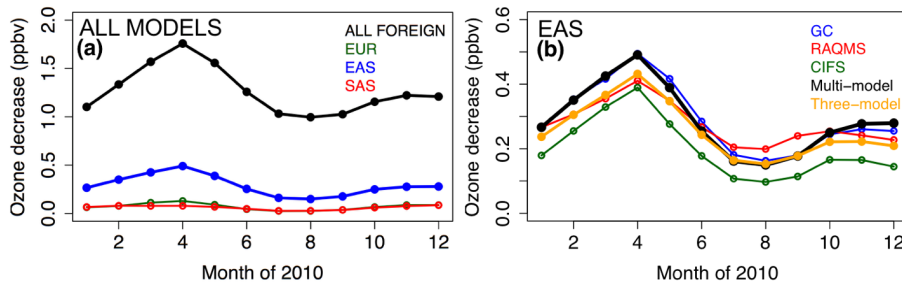
1526 **Figure 3.** (a) May-June 2010 period mean surface O₃ observations in ppbv at eight Japanese (filled
 1527 circles) and three Korean (filled triangles) EANET sites. (b) Observed and modeled monthly-mean
 1528 surface O₃ in 2010 at all eleven EANET sites. The “Multi-model” and “Three-model” in the legend
 1529 indicate the mean values of all eight global models and only of the three boundary condition
 1530 models, respectively.
 1531
 1532



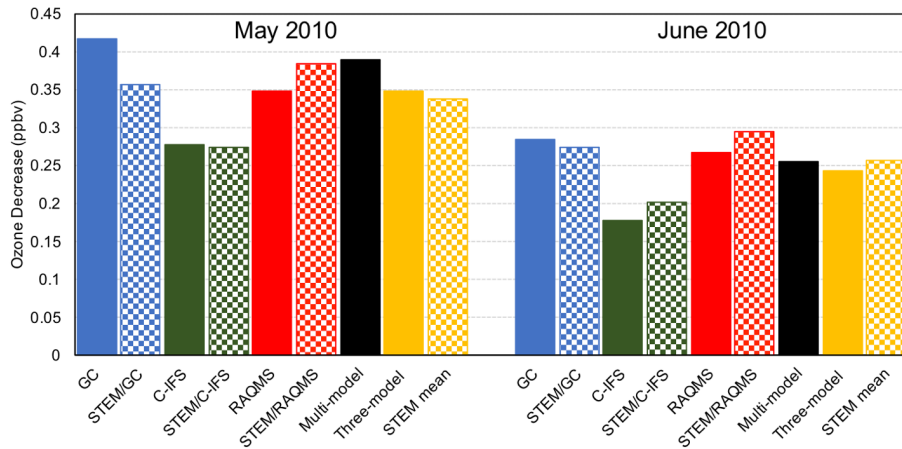
1533 **Figure 4.** Evaluation of the GEOS-Chem adjoint base NO₂ product (recorded at near the satellite
 1534 overpassing time) with the OMI NO₂ columns. The differences between OMI and GEOS-Chem
 1535 (OMI-modeled) tropospheric NO₂ columns ($\times 10^{15}$ molec./cm²) are shown for (a) May and (b) June
 1536 2010. Details of the comparison are included in Section 2.3.2.
 1537
 1538



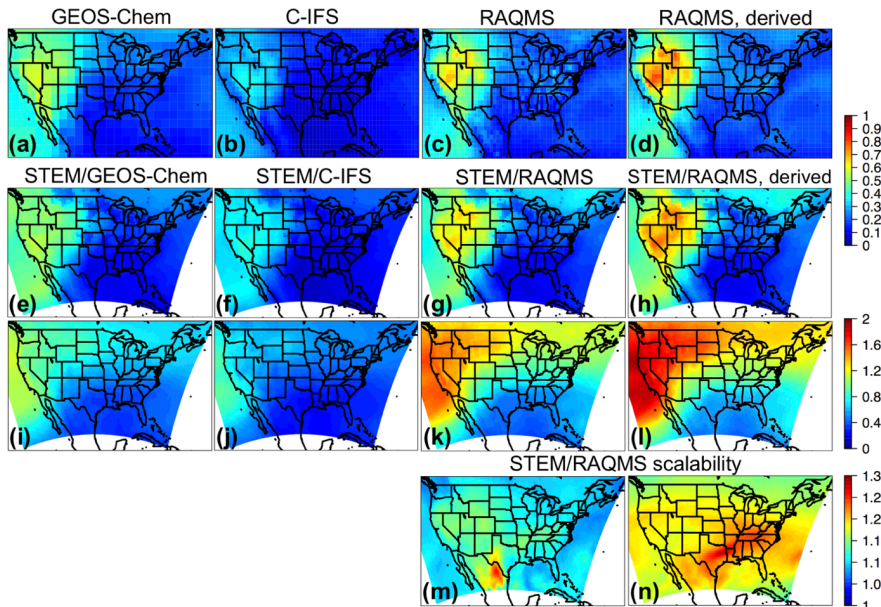
1539
 1540 **Figure 5.** The RERER maps in May (left) and June (right) 2010 over the continental US, calculated
 1541 based on the monthly mean O_3 from multiple global models' base and emission sensitivity
 1542 simulations. The RERER metric (unitless) was defined in eq. (2) in the text. Values larger than 1
 1543 and smaller than 0 are shown in purple and grey, respectively. The US (including continental US
 1544 as well as Hawaii which is not shown in the plots) mean values are indicated for each panel at the
 1545 lower right corner. All models show declining RERER values from May to June, and the 7-model
 1546 mean RERER values for May and June 2010 are ~ 0.5 and ~ 0.4 , respectively.



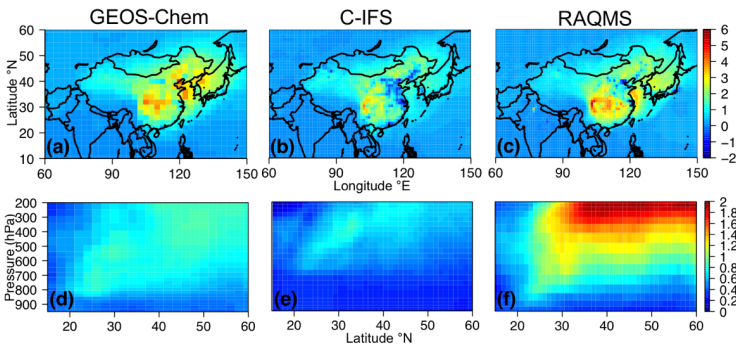
1547
 1548 **Figure 6. (a)** North American (130-65°W; 20-50°N) mean O₃ sensitivity to 20% anthropogenic
 1549 emission reductions in various non-North American regions, averaged from multiple (six-eight,
 1550 see details in text) global models. **(b)** North American surface R(O₃, EAS, 20%) values,
 1551 as estimated by single (the three STEM boundary condition models) or multi- global model means.
 1552 The “Multi-model” and “Three-model” in the legend indicate the mean sensitivities of all eight
 1553 global models and only of the three boundary condition models, respectively.
 1554



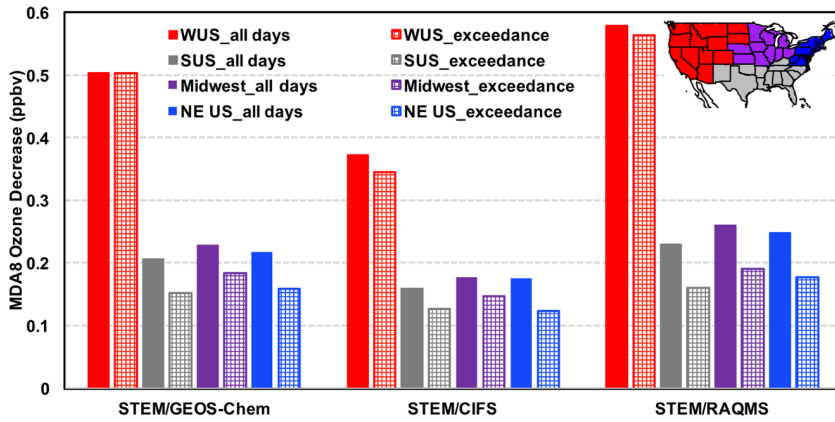
1555
 1556 **Figure 7.** Monthly-mean North American (130-65°W; 20-50°N) surface R(O₃, EAS, 20%) values
 1557 from multiple global and regional model simulations for May (left) and June (right) 2010. STEM
 1558 model mean values were calculated from its hourly output from 8 May and on. The “Multi-model”
 1559 and “Three-model” in the legend indicate the mean sensitivities of all eight global models and only
 1560 of the three boundary condition models, respectively.



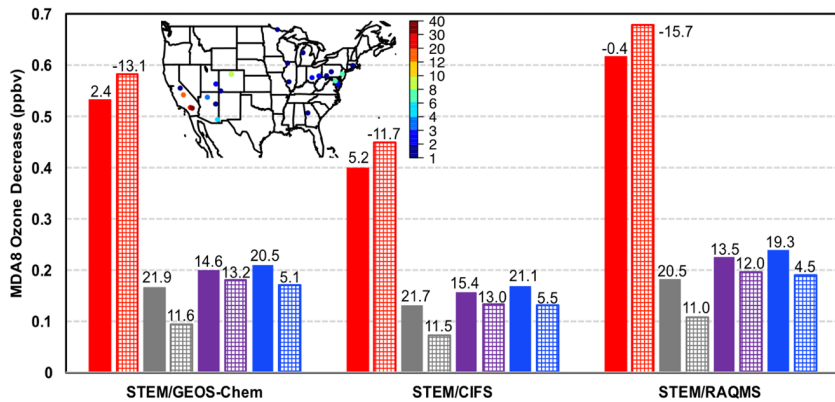
1561
 1562 **Figure 8.** The monthly-mean $R(\text{O}_3, \text{EAS}, 20\%)$ in June 2010 for: (a-d) surface O_3 (ppbv) from the
 1563 three boundary condition models, (e-h) STEM surface O_3 (ppbv), and (i-l) STEM column O_3
 1564 ($\times 10^{16}$ molecules/cm²). $R(\text{O}_3, \text{EAS}, 20\%)$ values from the simulations associated with GEOS-
 1565 Chem, ECMWF C-IFS, and RAQMS are shown in (a;e;i), (b;f;j) and (c;g;k), respectively. (d;h;l)
 1566 show 1/5 of the $R(\text{O}_3, \text{EAS}, 100\%)$ from the simulations related to RAQMS. STEM/RAQMS-
 1567 based “Scalability” S_{O_3} (eq. (3)) values over the NAM are shown for (m) surface and (n) column
 1568 O_3 .



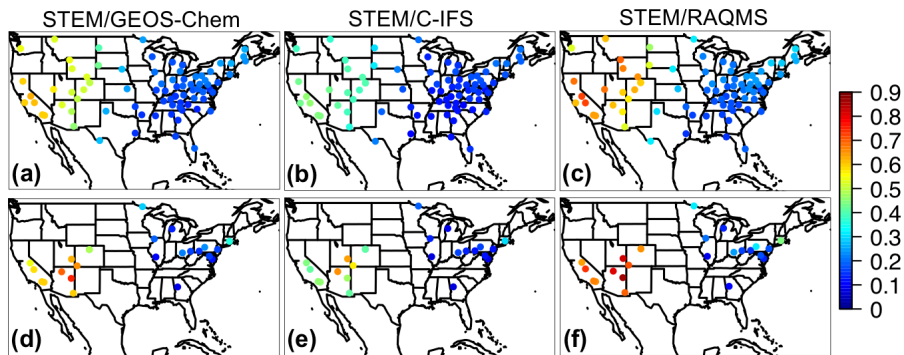
1569
 1570 **Figure 9.** The monthly-mean $R(\text{O}_3, \text{EAS}, 20\%)$ in ppbv in June 2010 from the three boundary
 1571 condition models at the source and near the receptor regions: (a-c) surface O_3 in the East Asia; and
 1572 (d) O_x (GEOS-Chem) or (e-f) O_3 (ECMWF C-IFS and RAQMS) along the cross section of 135°W
 1573 (near the west boundary of the STEM model domain as defined in Figure 2a).



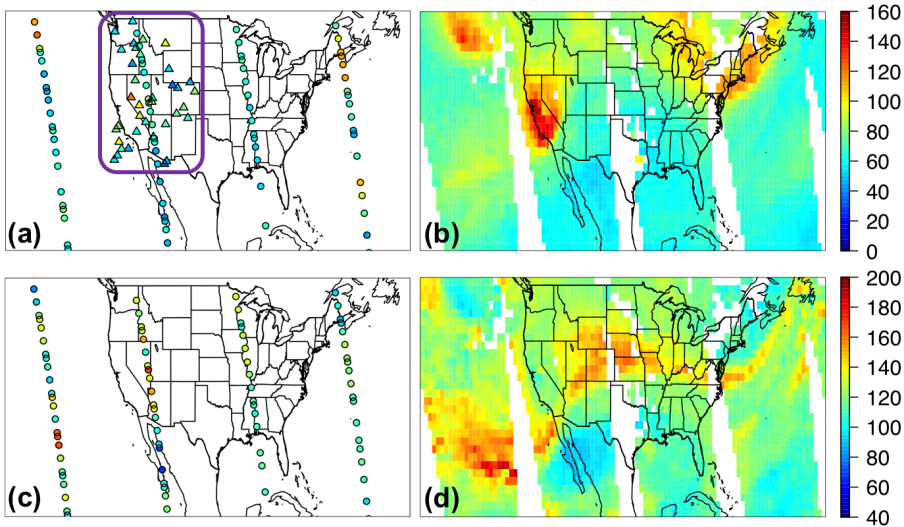
1574
 1575 **Figure 10.** STEM R(MDA8, EAS, 20%) for May-June 2010 in four US subregions (defined in the
 1576 inset panel, also consistent with the definitions in Figures 2/S4 and Tables 2-3), averaged on all
 1577 days (bars with solid fill) and only on the days when the simulated total MDA8 O₃ concentrations
 1578 were over 70 ppbv (bars with grid pattern fill). The results from the STEM runs using GEOS-
 1579 Chem, ECMWF C-IFS and RAQMS boundary conditions are shown separately.
 1580



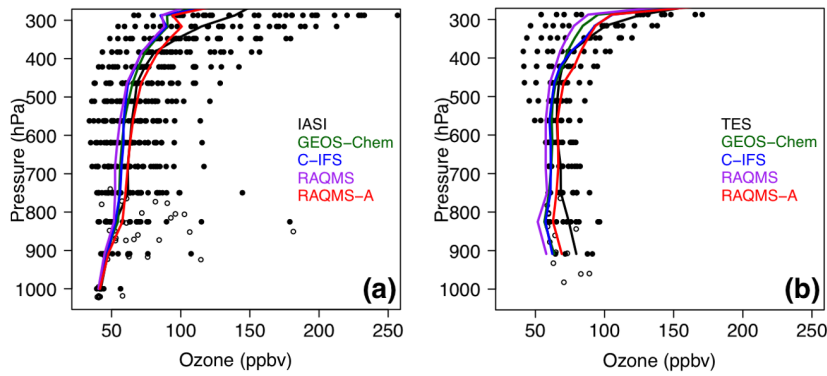
1581
 1582 **Figure 11.** STEM R(MDA8, EAS, 20%) for May-June 2010 at the CASTNET sites in four US
 1583 subregions (same definition as in Figure 10 inset), averaged on all days (bars with solid fill)
 1584 and only on the days when the observed MDA8 O₃ concentrations were over 70 ppbv (bars with
 1585 grid pattern fill). The results from the STEM runs using GEOS-Chem, ECMWF C-IFS and
 1586 RAQMS boundary conditions are shown separately. Biases for the corresponding model base runs
 1587 are shown above the bar plots. Inset shows at various CASTNET sites the number of days when
 1588 the observed MDA8 O₃ concentrations were over 70 ppbv.
 1589



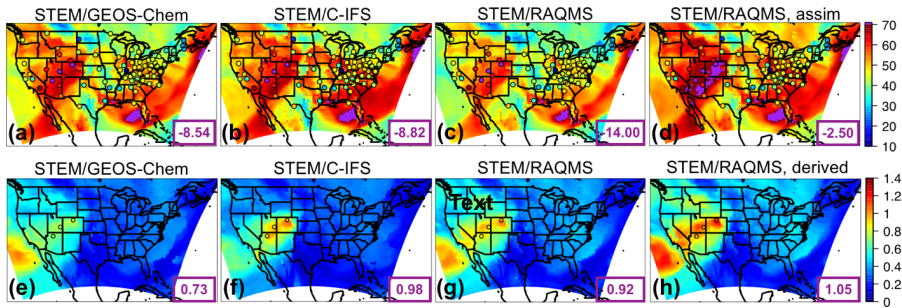
1590
 1591 **Figure 12.** STEM R(MDA8, EAS, 20%) in ppbv for May-June 2010 at the CASTNET sites on (a-
 1592 c) all days and (d-f) the days when the observed MDA8 O₃ concentrations were over 70 ppbv. The
 1593 results from the STEM runs using (a;d) GEOS-Chem, (b;e) ECMWF C-IFS and (c;f) RAQMS
 1594 boundary conditions are shown separately.
 1595



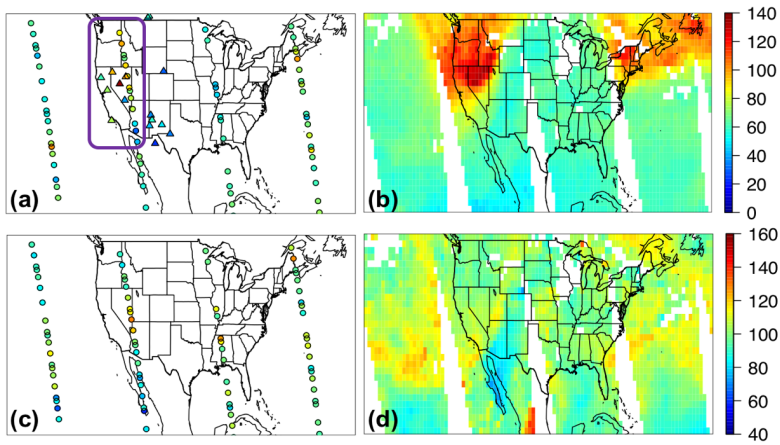
1596
 1597 **Figure 13.** Case study of 9 May 2010: (a-b) Ozone (ppbv) and (c-d) CO (ppbv) at ~500 hPa from
 1598 the L2 (a;c) TES retrievals (circles) and (b;d) L3 AIRS products at early afternoon local time. The
 1599 L2 IASI O₃ (ppbv) at ~500 hPa retrieved using the TES algorithm (details in Section 2.3.2) at the
 1600 mid- morning local times is shown on panel (b) as triangles. The O₃ profiles within the purple box
 1601 in panel (a) were used in the model evaluation shown in Figure 14.



1602
 1603 **Figure 14.** Case study of 9 May 2010: The comparisons between (a) IASI and (b) TES O₃ in the
 1604 western US with the simulated O₃ in the STEM runs using the GEOS-Chem (green), C-IFS (blue),
 1605 RAQMS (purple), and assimilated RAQMS (red) boundary conditions. The O₃ profiles within the
 1606 purple box in Figure 10a were used in the evaluation. Observation operators were applied in the
 1607 comparisons (details in Section 2.3.2). Solid and open dots are TES/IASI data at the TES retrieval
 1608 reporting levels and at the variable surface pressure levels, respectively. Solid lines are median O₃
 1609 profiles from the satellite observations and the different STEM simulations, calculated only on the
 1610 TES retrieval reporting levels.
 1611

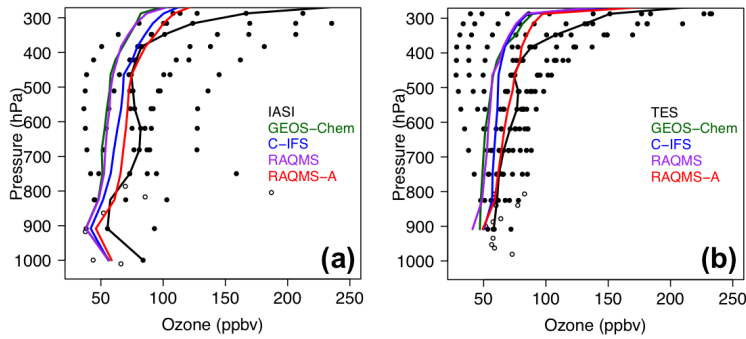


1612
 1613 **Figure 15.** Case study of 9 May 2010: (a-d) Surface MDA8 total O₃ and (e-h) surface R(MDA8,
 1614 EAS, 20%) from the STEM simulations using the (a;e) GEOS-Chem, (b;f) ECMWF C-IFS, and
 1615 (c;g) RAQMS free run as the boundary conditions. (d) Surface MDA8 total O₃ in a STEM base
 1616 simulation using the RAQMS assimilation run as the boundary conditions. CASTNET
 1617 observations are overlaid in filled circles in panels (a-d). (h) 1/5 of the surface R(MDA8, EAS,
 1618 100%) from STEM/RAQMS simulations. The conditions at ~400-500 hPa are shown in Figure S5.
 1619 Purple numbers at the lower right corners of (a-d) and (e-h) are mean model biases and mean
 1620 R(MDA8, EAS, 20%) values in ppbv at the three mountain sites (Grand Canyon NP, AZ;
 1621 Canyonlands NP, UT; and Rocky Mountain NP, CO) where O₃ exceedances were observed on this
 1622 day. The locations of these sites are shown in panel (e-h) as open circles.
 1623



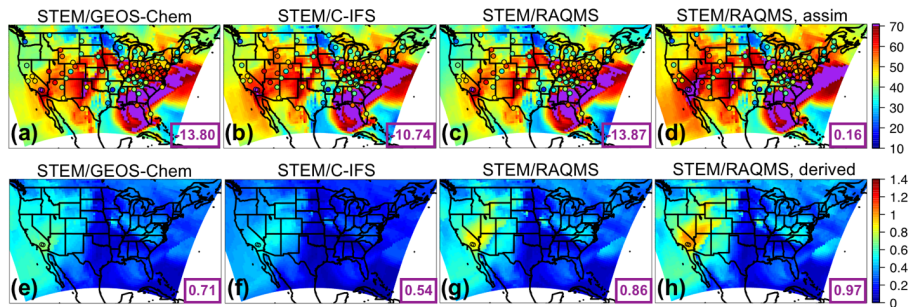
1624
1625
1626

Figure 16. Same as Figure 13, but for a case study of 10 June 2010.



1627
1628
1629

Figure 17. Same as Figure 14, but for a case study of 10 June 2010.



1630
1631
1632

Figure 18. Same as Figure 15, but for a case study of 10 June 2010. The CASTNET sites with O_3 exceedances on this day are Converse Station and Joshua Tree NP in southern California.

1633 **Table 1a.** HTAP2 base and sensitivity simulations by various global models. The STEM boundary
 1634 condition models are highlighted in bold.

Global model, Resolution: lon×lat×vertical layer, (References)	BASE	EASALL (-20%)	EASALL (-100%)	GLOALL (-20%)	NAMALL (-20%)	EURALL (-20%)	SASALL (-20%)
CAM-Chem, 2.5°×1.9°×56 (Tilmes et al., 2016)	✓	✓		✓	✓	✓	✓
CHASER T42, ~2.8°×2.8°×32 (Sudo et al., 2002)	✓	✓		✓	✓	✓	✓
EMEP rv48, 0.5°×0.5°×20 (Simpson et al., 2012)	✓	✓		✓	✓	✓	✓
SNU GEOS-Chem v9-01-03, 2.5°×2°×47 (Park et al., 2004; http://iek8wikis.iek.fz-juelich.de/HTAPWiki/WP2.3?action=AttachFile&do=view&target=_README_GEOS-Chem.pdf)	✓	✓		✓	✓		
CU-Boulder GEOS-Chem adjoint v35f, 2.5°×2°×47 (Henze et al., 2007)	✓	✓		✓	✓	✓	✓
RAQMS, 1°×1°×35, free running (Pierce et al., 2007, 2009)	✓	✓	✓				
RAQMS, 1°×1°×35, with satellite assimilation (Pierce et al., 2007, 2009)	✓						
OsloCTM3 v2, ~2.8°×2.8°×60 (Søvde et al., 2012)	✓	✓		✓	✓	✓	✓
ECMWF C-IFS, ~0.7°×0.7°×54/1.125°×1.1 25°×54, as the STEM chemical boundary conditions (Flemming et al., 2015)	✓	✓		✓	✓	✓	✓

Deleted: °×2

Deleted: °×2

- 1635 Acronyms:
 1636 CAM-Chem: Community Atmosphere Model with Chemistry
 1637 C-IFS: Composition-Integrated Forecasting System
 1638 ECMWF: European Center for Medium range Weather Forecasting
 1639 EMEP: European Monitoring and Evaluation Programme
 1640 GEOS-Chem: Goddard Earth Observing System with Chemistry
 1641 RAQMS: Realtime Air Quality Modeling System
 1642 SNU: Seoul National University

1645 **Table 1b.** STEM regional simulations for HTAP2

Boundary condition model, Resolution: lon×lat×vertical layer	BASE	EASALL (-20%)	EASALL (-100%)
SNU GEOS-Chem v9-01-03, 2.5°×2°×47	✓	✓	
RAQMS, 1°×1°×35, free running	✓	✓	✓
RAQMS, 1°×1°×35, with satellite assimilation	✓		
ECMWF C-IFS, 1.125°×1.125°×54	✓	✓	

Deleted: °×2

1646 **Table 1c.** STEM and its boundary condition models' key inputs and chemical mechanisms, with
1647 references. More details on the models can be found in Table 1a and the text.
1648

Model	Meteorology	Biogenic VOCs; NO _x	Lightning	Biomass Burning	Chemical Mechanism
GEOS- Chem	GEOS-5	MEGAN v2.1 (Guenther et al., 2012); Wang et al., 2009	based on GEOS-5 deep convective cloud top heights and climatological observations (Murray et al., 2012)	GFED v3.0 (van der Werf et al., 2010)	GEOS-Chem standard NO _x -O _x - hydrocarbon-aerosol (http://acmg.seas.harvard.edu/geos/doc/archive/man.v9-01-03/appendix_1.html)
RAQMS	Online (Pierce et al., 2007)				CB-IV (Gery et al., 1989) with adjustments
ECMWF C-IFS	IFS	MEGAN- MACC, (Sindelarova et al., 2014); POET database for 2000 (Granier et al., 2005)	based on IFS convective precipitation (Meijer et al., 2001)	GFAS v1.0 (Kaiser et al., 2012)	CB05 (Yarwood et al., 2005)
STEM	WRF-ARW v3.3.1	WRF- MEGAN v2.1	based on scaled WRF convective precipitation	FINN v1.0 (Wiedinmyer et al., 2011)	SAPRC99 (Carter, 2000)

1649 Acronyms:

1650 CB: Carbon Bond

1651 FINN: Fire INventory from NCAR

1652 GFAS: Global Fire Assimilation System

1653 GFED: Global Fire Emissions Database

1654 IFS: Integrated Forecasting System

1655 MACC: Monitoring Atmospheric Composition and Climate

1656 MEGAN: Model of Emissions of Gases and Aerosols from Nature

1657 POET: Precursors of Ozone and their Effects in the Troposphere

1658 WRF-ARW: Advanced Research Weather Research and Forecasting Model

1660 **Table 2a.** Evaluation of the period mean (1 May-30 June, 2010) multi- global model free
 1661 simulations against the CASTNET observations, only at the sites where 95% of the hourly O₃
 1662 observations are available. Evaluation of the individual models is summarized in Table 2b.

Subregion	US EPA regions contained	Number of sites	Mean bias (ppbv)		RMSE (ppbv)	
			3 BC ^a models	8 global models	3 BC models	8 global models
Western US	8, 9, 10	19	-5.68	-2.52	10.37	7.05
Southern US	4, 6	18	11.61	10.24	13.62	11.96
Midwest	5, 7	13	8.03	7.66	9.16	8.67
Northeast	1, 2, 3	17	9.55	10.63	10.28	11.24
All	1-10	67	5.49	6.22	11.11	9.96

^aBC: Boundary Conditions

1663
 1664
 1665
 1666
 1667

Table 2b. Evaluation of the period mean (May-June 2010) global model free simulations against the EANET and CASTNET observations. The STEM boundary condition models are highlighted in bold.

Network	Number of sites	RMSE (ppbv)							
		CAM-Chem	EMEP	CHASER	SNU GEOS- Chem	GEOS-Chem adjoint	RAQMS	OsloCTM3 v2	C-IFS
CASTNET	67	13.30	11.61	15.43	15.55	13.48	9.32	11.05	11.00
EANET	11	10.38	9.96	11.39	9.18	11.04	8.60	12.97	10.86

1668
 1669
 1670
 1671

Table 2c. Evaluation of the period mean (May-June 2010) multi- global model free simulations against the EANET observations in Japan and Korea. Evaluation of the individual models is summarized in Table 2b.

Country	Number of sites	Mean bias (ppbv)		RMSE (ppbv)	
		3 BC ^a models	8 global models	3 BC models	8 global models
Japan	8	0.36	1.01	8.77	9.25
Korea	3	1.14	3.98	8.37	10.51
All	11	0.57	1.82	8.66	9.61

^aBC: Boundary Conditions

1672

1673 **Table 3a.** Evaluation of the hourly STEM simulated total O₃ (averaged from the three base
 1674 simulations that used the different free-running boundary conditions) against the CASTNET
 1675 surface observations for 8 May-30 June, 2010. The subregional mean R(O₃, EAS, 100%) and its
 1676 correlation coefficient with the observed O₃ are also shown.

Subregion	US EPA regions contained	Number of sites	Mean elevation (km): actual/model	Mean bias (ppbv)	RMSE (ppbv)	Correlation (model base; obs)	Correlation (obs; modeled EAS)	Mean EAS sensitivity (ppbv)
Western US	8, 9, 10	22	1.75/ 1.71	1.60	4.86	0.76	0.34	0.48
Southern US	4, 6	22	0.38/ 0.31	20.33	22.13	0.58	0.27	0.15
Midwest	5, 7	16	0.29/ 0.28	15.64	17.97	0.70	0.15	0.17
Northeast	1, 2, 3	20	0.36/ 0.26	20.94	24.16	0.47	0.17	0.21
All	1-10	80	0.73/ 0.68	16.17	18.30	0.66	0.13	0.20

1677 **Table 3b.** Evaluation of the hourly STEM simulated total O₃ (separately for three base simulations
 1678 that used the different free-running boundary conditions) against the CASTNET surface
 1679 observations for 8 May-30 June, 2010.
 1680

Subregion	US EPA regions contained	Number of sites	Mean bias (ppbv)/RMSE (ppbv)/Correlation (model base; obs)		
			SNU GEOS-Chem	C-IFS	RAQMS
Western US	8, 9, 10	22	1.68/4.83/0.77	4.16/6.63/0.70	-1.03/4.81/0.76
Southern US	4, 6	22	21.18/22.94/0.57	20.34/22.07/0.60	19.48/21.45/0.56
Midwest	5, 7	16	15.77/18.17/0.70	16.41/18.46/0.72	14.73/17.35/0.69
Northeast	1, 2, 3	20	21.25/24.36/0.47	21.86/24.80/0.48	19.71/23.40/0.45
All	1-10	80	16.57/18.62/0.66	16.89/18.84/0.67	15.03/17.52/0.64

1681

1682 **Table 4.** The ranges and standard deviations (ppbv, separated by “;”) of R(O₃, *source region*, 20%)
 1683 by 6-8 global models (defined in eq. (1a-d)), summarized by months in 2010. The monthly multi-
 1684 model mean values are shown in Figures 5-6.

Month/ Source region	All Foreign/ Non-NAM (ppbv)	EUR (ppbv)	EAS (ppbv)	SAS (ppbv)
Jan	0.38-1.69; 0.41	0.002-0.12; 0.05	0.02-0.72; 0.24	0.001-0.11; 0.04
Feb	0.92-2.07; 0.37	0.02-0.15; 0.05	0.16-0.91; 0.28	0.02-0.12; 0.04
Mar	1.30-2.37; 0.38	0.07-0.21; 0.06	0.24-1.03; 0.30	0.03-0.12; 0.03
Apr	1.42-2.46; 0.33	0.09-0.23; 0.05	0.33-1.07; 0.28	0.04-0.12; 0.03
May	1.24-1.91; 0.21	0.06-0.17; 0.04	0.24-0.75; 0.19	0.05-0.11; 0.02
Jun	1.03-1.41; 0.13	0.03-0.07; 0.02	0.14-0.39; 0.09	0.04-0.07; 0.01
Jul	0.86-1.18; 0.13	0.02-0.04; 0.01	0.08-0.22; 0.06	0.01-0.04; 0.01
Aug	0.80-1.19; 0.13	0.01-0.04; 0.01	0.07-0.20; 0.05	0.02-0.04; 0.01
Sep	0.85-1.18; 0.13	0.03-0.05; 0.01	0.10-0.25; 0.06	0.02-0.06; 0.01
Oct	0.96-1.31; 0.14	0.04-0.10; 0.02	0.17-0.42; 0.09	0.03-0.08; 0.02
Nov	0.90-1.48; 0.19	0.05-0.15; 0.04	0.17-0.54; 0.14	0.04-0.10; 0.02
Dec	0.73-1.67; 0.29	0.03-0.18; 0.05	0.14-0.66; 0.19	0.04-0.12; 0.03

1685